







## Article

# Removal of Ethyl Xanthate Anions from Contaminated Aqueous Solutions Using Hazardous Waste Slag Generated by Lignite Combustion

Andrijana Vasić<sup>1</sup>, Jelena Gulicovski<sup>1</sup>, Marija Stojmenović<sup>1</sup>, Neda Nišić<sup>1</sup>, Katarina Nikolić<sup>1</sup>, Ivona Nuić<sup>2</sup> and Milan Kragović<sup>1,\*</sup>

<sup>1</sup> “VINČA”, Institute of Nuclear Sciences, National Institute of the Republic of Serbia, University of Belgrade, Mike Petrovića Alasa 12-14, 11351 Belgrade, Serbia

<sup>2</sup> Department of Environmental Engineering, Faculty of Chemistry and Technology, University of Split, Rudera Boškovića 35, 21000 Split, Croatia

\* Correspondence: m.kragovic@vin.bg.ac.rs

**Abstract:** This paper presents the results of the application of hazardous waste slag generated by lignite combustion for the adsorption of ethyl xanthate anions (EX) from aqueous solutions. The starting material (RWS) was washed (WWS) and modified (MWS) and then characterized in detail by using different chemical and physical–chemical techniques (determination of chemical composition and content of heavy metals, X-ray diffraction (XRD), infrared spectroscopy (FTIR), determination of textural properties and point of zero charge). Besides the chemical stability of EX, the influence of the initial pH, mass of the adsorbent, initial concentration, and time on the EX anion removal was tested. The characterization results showed that applied waste slag is a hazardous material with complex mineral and structural properties but with good buffer properties and pH stability, which is also characteristic of the MWS sample. The adsorption experiments showed that modification with  $\text{Cu}(\text{NO}_3)_2$  and  $\text{Fe}(\text{NO}_3)_3$  significantly increases the adsorption capacity of the starting slag. Under applied experimental conditions, the maximal adsorbed amount of EX anions on the MWS was 210 mg/g, while equilibrium was obtained after 700 min. The Freundlich model and pseudo-second-order model best fit the results, suggesting the complex mechanism of EX removal by the MWS sample.

**Keywords:** practical application of hazardous waste; slag from lignite combustion; ethyl xanthate; adsorption; removal mechanism



**Citation:** Vasić, A.; Gulicovski, J.; Stojmenović, M.; Nišić, N.; Nikolić, K.; Nuić, I.; Kragović, M. Removal of Ethyl Xanthate Anions from Contaminated Aqueous Solutions Using Hazardous Waste Slag Generated by Lignite Combustion. *Water* **2024**, *16*, 2037. <https://doi.org/10.3390/w16142037>

Academic Editor: Andreas Angelakis

Received: 19 June 2024  
Revised: 15 July 2024  
Accepted: 16 July 2024  
Published: 18 July 2024



**Copyright:** © 2024 by the authors. Licensee MDPI, Basel, Switzerland. This article is an open access article distributed under the terms and conditions of the Creative Commons Attribution (CC BY) license (<https://creativecommons.org/licenses/by/4.0/>).

## 1. Introduction

In recent years, several problems related to the disposal of large amounts of waste produced by human activities or industry have been emerging. Therefore, there is a strong tendency of modern society and the scientific community to move to approaches that are aimed at the minimization or even elimination of waste. As one of the major principles of the circular economy, the conversion of waste into useful secondary products became an ultimate objective of current research [1,2]. Hence, to find proper sustainable solutions, researchers are now frequently looking for alternative potential purposes for various industrial waste and by-products.

Slag is a waste product that is mostly generated in the steel-making industry, in metal smelting processes, or by incomplete combustion of coal such as lignite. It usually stands as a solid-state, long-lasting waste material with uniformly sized particles highly resistant to surface wear [3,4].

Waste slag is usually considered a hazardous waste product because of dangerous levels of heavy metals in the composition, such as cadmium, arsenic, or zinc, as well as other unfavorable substances, which are threatening the environment and affecting human

health [3]. Each year, millions of tons of slag are disposed of in landfills worldwide, of which only Serbia generates more than one million tons [5].

The research focused on finding the potential utility of hazardous waste slag is still in the beginning since there are only a few studies related to this field so far. In our previous studies [3,6], waste slag generated by lignite combustion in a heating plant in Serbia was tested for application in concrete and mortar production. Further, in very few research papers, waste slags of different origins were investigated as adsorbents for different contaminants of certain wastewater [7,8]. For example, in the research conducted by Ma et al. [7], waste slag composite in the form of electrolytic manganese residue was thermally activated with calcite in order to obtain silicone-based adsorbent. This material was studied for the removal of cadmium and lead ions from polluted water. The results have shown that it could be adopted as an eco-friendly, low-cost, and highly efficient adsorbent for heavy metal ions, whereby, besides adsorption, both ion exchange and precipitation have been found responsible for successful heavy metal ions removal. The results indicate that the removal efficiency for  $\text{Cd}^{2+}$  was almost 80% in the pH range from 2 to 7 for the initial  $\text{Cd}^{2+}$  concentration of  $300 \text{ mg/dm}^3$ , while for  $\text{Pb}^{2+}$ , it was 92% in the pH range from 1 to 4 for the initial  $\text{Pb}^{2+}$  concentration of  $610 \text{ mg/dm}^3$ .

Hashim et al. [8] attempted to develop an innovative adsorbent based on waste slag from steel-making industries in order to capture carbon dioxide ( $\text{CO}_2$ ) present in contaminated waters. Adsorbents were prepared with an addition of various acids, whereby the one synthesized using formic acid showed the highest  $\text{CO}_2$  adsorption capacity (17 wt%) and the best regenerative ability, as well.

The xanthates (Figure 1) are salts or esters of xanthic acid. The general formula of the salt of xanthic acid is  $[\text{R}-\text{O}-\text{CS}_2]^- \text{M}^+$  (where R is the organic group, and M is usually Na or K) [9]. Xanthates are generally known as one of the most common reagents used in the flotation process as collectors in the separation of gold ores, as well as sulfidic metal ores, and therefore largely present in flotation wastewater as residuals [10,11]. Common xanthate products used for the purpose of mineral processing are sodium ethyl xanthate, potassium ethyl xanthate, sodium isopropyl xanthate, sodium isobutyl xanthate, and potassium amyl xanthate. In practice, a group of xanthate compounds is considered crucial in the flotation of sulfide minerals, and their application is inevitable for achieving the required efficiency and selectivity of these processes [12]. Although there are tendencies to avoid the use of xanthates for these technological operations and to replace them with green, environmentally friendly alternatives, they are still the most widely used. Moreover, their consumption is even increasing on a global scale. For instance, only in the mining sector did global consumption of xanthates amount to around 52,000 tons per year in the 80s, and since then, it has been continuously growing. Moreover, its annual consumption is estimated to reach approx. 372,000 tons by the year 2025 [13]. Currently, the average consumption of xanthate is  $\sim 10 \text{ g/0.1 wt\%}$  of metal empirically. Even though xanthates are applied for the extraction of valuable minerals from the ore, considering technological limits, a great amount remains in the tailings that have to be disposed of in the environment.

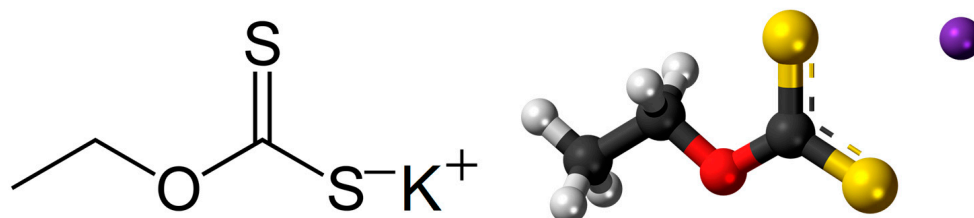


**Figure 1.** Structural and ball-and-stick model of the potassium-ethyl xanthate molecule. ●—carbon; ●—hydrogen; ●—oxygen; ●—potassium, ●—sulfur.

In a chemical sense, the xanthates consist of a hydrocarbon nonpolar radical part and a polar group [14]. Residual xanthates and other by-products of their decomposition remain in wastewater and can be extremely dangerous and toxic even at very low concentrations

(<1 mg/dm<sup>3</sup>) for human health and flora and fauna in the surrounding of the mining areas, while according to the EPA (Environmental Protection Agency) for disulfates, which include xanthates, the discharge limit is 1 ppm for a period of 8–10 h. Xanthates can accumulate in living organisms and enhance heavy metal augmentation, causing various diseases and adverse effects on human physiological functions [15]. The effects of xanthates on human health are usually neurological or/and reproductive, as well as cardiovascular disease, systemic ophthalmological effects, damaging the blood vessels of the retina, and (at higher exposures) increased mortality from heart disease [11,16]. Flotation tailings are, therefore, regarded as extremely harmful waste routes. Thus, it is essential to develop additional proper techniques for the purification of wastewater contaminated with xanthates originating mainly from the mining industry.

Since there is a lack of effective techniques that are successfully applied for the removal of xanthates from industrial wastewater, there is a tendency toward the investigation of innovative, practical methodologies for that purpose. According to different reports in the literature [17–23], mining wastewater treatment processes have been studied extensively in terms of xanthates removal so far. Different degradation mechanisms were proposed, such as photocatalytic [18,19] and biological [17]. Nevertheless, adsorption seems to present the most effective and easiest method, but also a low-cost solution for such treatment, especially if some eco-friendly secondary materials are applied as adsorbents. Various adsorbents with high efficiency for the treatment of xanthate-contaminated wastewater have been suggested by researchers recently. The successful removal of potassium ethyl xanthate from wastewater was performed in the work of Panayotova et al. [20], where silver nanoparticles and zeolite composites were used for that purpose. From the obtained results, over 75% of xanthate was removed in the time of 120 min using the prepared AgNPs zeolite for an initial xanthates concentration of 20 mg/dm<sup>3</sup>, while the complete removal of xanthate was reached in 60 min at concentrations lower than 1 mg/dm<sup>3</sup> at the initial pH of 7. Also, in the study of Rezaei et al. [21], modified bentonite was used as an adsorbent for the xanthates from the flotation tailings. The modification consisted of bentonite activation using mineral acids. The authors conducted tests with an adsorbent mass of 7500 mg/dm<sup>3</sup> and a xanthate concentration of 2000 mg/dm<sup>3</sup>. It was concluded that aluminum-pillared (Al-Be) had a higher adsorption capacity for xanthate compared to acid-activated (H-Be), where the best xanthate removal (99%) was achieved at pH = 12.2 after 45 min. A similar examination was reported in the paper of Amrollahi et al. [22], where tests were conducted with a mass of adsorbent of 4 mg/dm<sup>3</sup> at an initial concentration of xanthate of 1000 mg/dm<sup>3</sup> at pH = 9.2. It was established that bentonite modified with copper (Be-CuFe<sub>2</sub>) had a high adsorption capacity for xanthate, and more than 94% of xanthate was removed from the solution after 40 min.

According to the literature review so far, some studies have only referred to the potential application of waste slag from the steel-making industry. What is more, such slag has been successfully examined and applied for the adsorption of different contaminants from polluted water, such as heavy metals (lead, cadmium, arsenic, copper, etc.), organic pollutants (organic aromatic compounds, phenolic compounds, pesticides...), synthetic chemicals, toxic microorganisms, suspended particles, etc. [24].

However, there is still a lack of research on waste slag originating from the mining industry or the lignite combustion processes for the same or similar purposes. Since this kind of slag has a great potential for utilization, considering the good performance of the waste slag from other industries, and since it is becoming widely present and growing global concern in numerous power plants in Serbia, but also globally, we have taken the initiative to cover that gap. Therefore, in this study, we investigated the possibility of the potential application of the waste slag obtained as a by-product from lignite combustion for the effective treatment of wastewater contaminated with ethyl xanthate. In order to improve adsorption properties and achieve high adsorption efficiency, waste slag was initially washed with distilled water, then modified using iron and copper salts and tested for the removal of ethyl xanthate anions from simulated aqueous solutions. During exper-

iments, the influence of adsorbent mass, initial pH, and ethyl xanthate concentration on the adsorption process was thoroughly examined. Afterward, the kinetic of ethyl xanthate removal was studied, as well. Furthermore, the characterization of the waste slag was performed using different physical–chemical and instrumental methods.

The main objective of this study was to determine the optimal conditions for the removal of ethyl xanthate anions from simulated wastewater by modified waste slag from lignite combustion processes, to provide an explanation for the adsorption mechanism, and thereby to confirm its applicability for this purpose. This would represent a complete reduce certain expenses and issues concerning its disposal in landfills and environmental endangerment. Also, a new value-added product, potentially efficient and ecologically acceptable, would be provided. What is more, the principles of sustainable development and zero-waste living would be complied with, which is practically the ultimate goal of the current research in the field.

## 2. Materials and Methods

### 2.1. Sampling

The raw waste slag (RWS) (Figure 2) was from an industrial landfill in Valjevo, Serbia. The samples were taken from six different places at three different depths, representing a total of 30 samples. Thereafter, the samples were dried at 105 °C, then homogenized and ground so that the particle size was 100% lower than 63 µm. After grinding, the slag was rinsed several times with distilled water until a clear aqueous filtrate was obtained and pH reached 7. The washed waste slag (WWS) was then modified using copper and iron salts.



**Figure 2.** Raw (left) and modified waste slag sample (right).

### 2.2. Modification of Waste Slag with Magnetic Nanoparticles

The WWS sample was modified by following the procedure [22]. The 5 g of  $\text{Cu}(\text{NO}_3)_2 \times 3\text{H}_2\text{O}$  and 16 g of  $\text{Fe}(\text{NO}_3)_3 \times 9\text{H}_2\text{O}$  were dissolved in 400 cm<sup>3</sup> distilled water and stirred for 20 min. The 5 g of washed waste slag was added to the suspension and stirred for an additional 30 min on a magnetic stirrer. The pH was adjusted to 10 by adding the 5 mol/dm<sup>3</sup> NaOH in drops, and then the suspension was heated at 100 °C for 2 h. Finally, the suspension was filtered, and the supernatant was washed several times with distilled water in order to remove excess nitrate ions and dried at 105 °C. The final sample (MWS) was then ground again so that the particle size was 100% lower than 63 µm (Figure 2).

### 2.3. Characterization

#### 2.3.1. Chemical Analysis

The chemical composition and heavy metal content of the RWS were determined by classical chemical analysis [3,25]. Measuring was performed on atomic absorption spectrophotometry on instruments AAnalyst 300 (Analytic Jena, Jena, Germany) and Specol 1300 (Analytic Jena, Jena, Germany).

### 2.3.2. X-ray Diffraction Analysis (XRD)

The crystal-phase analyses of slag samples RWS, WWS, and MWS were determined by X-ray diffraction (XRPD) method using an Ultima IV Rigaku diffractometer (Rigaku International Corporation, Tokyo, Japan) equipped with  $\text{CuK}\alpha_{1,2}$  radiation. For all slag samples,  $2\theta$  in the range of  $5\text{--}90^\circ$  was used in a continuous scan mode with a scanning step size of  $0.02^\circ$  and at a scan rate of  $0.5^\circ/\text{min}$ . The PDXL2 (Ver. 2.8.4.0) software was used for phase identification [26]. All obtained phases were identified using the ICDD crystallographic database [27]. The following PDF card numbers were used for phase identifications: 01-087-2096 ( $\text{SiO}_2$ -quartz), 00-007-0158 ( $(\text{Fe, Mg})_2\text{SiO}_4$ -olivine), 00-041-1480 ( $(\text{Ca, Na, K})(\text{Si, Al})_4\text{O}_8$ -feldspar), 05-001-0465 ( $\text{SiO}_2$ -trydimite), 00-001-1295 ( $\text{FeS}_2$ -pyrite), and 01-080-6409 ( $\text{Fe}_3\text{O}_4$ -magnetite).

### 2.3.3. Infrared Spectroscopy with Fourier-Transform (FTIR)

FTIR analyses of the RWS, WWS, and MWS were performed on a Perkin Elmer Spectrum Quant instrument (Beaconsfield, UK). The samples were finely ground and dispersed with anhydrous KBr (1:100) in order to form pellets. Recording of the spectra was carried out in the range of  $4000\text{--}400\text{ cm}^{-1}$  by using the DRIFT technique. The resolution was  $2\text{ cm}^{-1}$ , while the number of scans was 64. After recording, baseline correction and atmospheric correction were performed to eliminate the influence of the  $\text{CO}_2$  and  $\text{H}_2\text{O}$ .

### 2.3.4. Textural Properties

The textural properties of the MWS sample were determined on the instrument Surfer (Thermo Fisher Scientific, Waltham, MA, USA). The adsorption–desorption isotherms of nitrogen were obtained at  $-196^\circ\text{C}$ . During the adsorption test, the sample was first degassed for 1 h at room temperature and then for 16 h at  $110^\circ\text{C}$  under the same pressure. ADP version 5.13 Thermo Electron software was used for isotherm analysis. The Brunauer–Emmett–Teller (BET) method was used to determine the specific surface area ( $S_{\text{BET}}$ ) [28]. The total pore volume ( $V_{\text{tot}}$ ) was given at  $p/p^\circ = 0.95$ . The volume of the mesopores was calculated according to the mesopore (Cranston and Inkley) method [29]. The volume of micropores was calculated from the alpha-S plot [30,31].

### 2.3.5. The Point of Zero Charge ( $\text{pH}_{\text{pzc}}$ )

For determination of the  $\text{pH}_{\text{pzc}}$  for all waste samples—RWS, WWS, and MWS—the methodology previously described in the literature [32,33] was applied. A total of 100 mg of each sample was weighed in 10 Erlenmeyer flasks and poured into  $50\text{ cm}^3$  of  $\text{KNO}_3$  solutions of different concentrations (0.1, 0.01, and  $0.001\text{ mol/dm}^3$ ). The initial pHs ( $\text{pH}_i$ ) were set in the range of 2–12 by adjusting with  $\text{HNO}_3$  ( $0.1\text{ mol/dm}^3$ ) or  $\text{KOH}$  ( $0.1\text{ mol/dm}^3$ ) solutions. The obtained suspensions were continually stirred for 24 h at  $25^\circ\text{C}$  on an orbital shaker at 250 rpm. Afterward, suspensions were centrifuged, and the final pHs ( $\text{pH}_f$ ) of each filtrate were measured. The point of zero charge was determined as a plateau on the diagram,  $\text{pH}_f = f(\text{pH}_i)$ .

## 2.4. Adsorption Experiments

### 2.4.1. Chemical Stability of Ethyl Xanthate in Aqueous Solution

Before the investigation of the ethyl xanthate (EX) removal, its stability in the pH range of 2–12 (adjusted using  $0.1\text{ mol/dm}^3\text{ HNO}_3$  or  $0.1\text{ mol/dm}^3\text{ KOH}$ ) was investigated during 30 h at  $25^\circ\text{C}$ . The EX concentration in a solution of  $20\text{ mg/dm}^3$  was analyzed in a volume of  $50\text{ cm}^3$  in 6 Erlenmeyer flasks. The ethyl xanthate concentration was measured using UV-VIS spectrometer SHIMADZU UV-1900 (Shimadzu, Kyoto, Japan) at wavelengths of 200 and 400 nm.

### 2.4.2. Initial Test of the EX Anion Removal

The RWS, WWS, and MWS samples were initially tested for the removal of EX from polluted aqueous solutions. The initial EX concentration was  $20\text{ mg/dm}^3$ , the adsorbent

mass was 10 mg, and reaction volume was 50 cm<sup>3</sup> over 24 h at pH<sub>i</sub> = 10 and 25 °C. The suspensions were continuously stirred at 250 rpm. After the reaction time, the suspensions were centrifuged, after which residual concentrations of ethyl xanthate were measured on a UV-VIS spectrometer.

#### 2.4.3. Influence of pH<sub>i</sub> on the Removal of EX Anions

The pH influence of the EX anion removal using the MWS sample was tested as follows: ten Erlenmeyer's were used; in each one, 10 mg of MWS was put and overflowed with 50 cm<sup>3</sup> of solution with EX concentration of 20 mg/dm<sup>3</sup>. Desired pHs in the range of 8–12 were obtained by the addition of 0.1 mol/dm<sup>3</sup> KOH. Suspensions were shaken for 24 h at 25 °C, and then the suspensions were centrifuged. Initial and residual concentrations of EX (after adsorption) were determined by UV-VIS spectrometry.

#### 2.4.4. Influence of Adsorbent Mass on the EX Anion Removal

The influence of the mass of the adsorbent on the EX anion removal using MWS was tested as follows: ten Erlenmeyer's of 100 cm<sup>3</sup> were used; in each, a different mass of MWS sample (1–500 mg) was placed and poured with 50 cm<sup>3</sup> of 100 mg/dm<sup>3</sup> EX solution. The pH<sub>i</sub> of all samples was set to 10 by adding 0.1 mol/dm<sup>3</sup> KOH. The suspensions were shaken 24 h, at 250 rpm and at 25 °C. Then, the suspensions were centrifuged, and the final EX concentrations were determined on a UV-VIS spectrometer at λ = 301 nm.

#### 2.4.5. Effect of EX Anions Concentration on Removal Efficiency of the MWS

The impact of the initial pollutant's concentration was studied at different concentrations of EX (10–100 mg/dm<sup>3</sup>), at pH<sub>i</sub> = 10, for the mass of adsorbent of 10 mg in the volume of 50 cm<sup>3</sup>. The suspensions were shaken at 250 rpm at 25 °C for 24 h. After that, the suspensions were centrifuged for 10 min at 10,000 rpm.

The obtained results were fitted according to the three most frequently used adsorption models (Langmuir, Freundlich, and Temkin model) [34]. The Langmuir model is used to define the monolayer adsorption on the homogenous surface of the adsorbent. The Langmuir isotherm can be represented by the following equation [35]:

$$q_e = \frac{bq_{\max}C_e}{1 + bC_e} \quad (1)$$

Or they can be represented in linear form:

$$\frac{1}{q_e} = \frac{1}{q_{\max}} + \frac{1}{bq_{\max}} \frac{1}{C_e} \quad (2)$$

where  $q_{\max}$  represents the maximum adsorption capacity (mg/g),  $C_e$  is the equilibrium concentration of EX (mg/dm<sup>3</sup>),  $b$  is the Langmuir constant related to the heat of the adsorption (dm<sup>3</sup>/mg), and  $q_e$  (mg/dm<sup>3</sup>) is the adsorbed amount of EX.

The Freundlich model is used to describe the multilayer adsorption on heterogeneous surfaces [36]. The Freundlich isotherm is given in the following equation:

$$q_e = K_F C_e^{1/n} \quad (3)$$

In the linear form, it is

$$\log q_e = \log K_F + 1/n \log C_e \quad (4)$$

where  $K_F$  (dm<sup>3</sup>/mg) and  $n$  are Freundlich constants, respectively, while  $1/n$  is the surface heterogeneity factor.

The Temkin adsorption isotherm can be presented with the following equation [37]:

$$q_e = \frac{RT}{b} \ln(K_t C_e) \quad (5)$$

where  $R$  is the gas constant (8.314 J/mol K),  $T$  is the temperature (K), and  $b$  is Temkin's constant, which refers to the heat of adsorption (J/mol). Also,  $K_t$  is Temkin's constant ( $\text{dm}^3/\text{mg}$ ), and  $C_e$  is the equilibrium concentration ( $\text{mg}/\text{dm}^3$ ) [38].

#### 2.4.6. Kinetic of the EX Anion Removal

The adsorption kinetic was investigated for the initial concentrations of  $50 \text{ mg}/\text{dm}^3$  EX were used. The solid/liquid ratio for these experiments was  $10 \text{ mg}/50 \text{ cm}^3$ . Experiments were conducted at  $25^\circ\text{C}$  at  $\text{pH}_i = 10$ . The 10 Erlenmeyer flasks were used (one Erlenmeyer flask for each time interval) so that in each of them, an appropriate suspension of adsorbent and EX solution was made, and then, at a certain time in 0–24 h interval, the suspensions were filtered using a vacuum pump (the time required for filtration and separation of the liquid and solid phases was about 15 s), and then residual EX concentrations were analyzed.

The results obtained from the investigation of the kinetics of EX removal on the MWS were fitted with four kinetic models: pseudo-first-order, pseudo-second-order, Boyd, and Weber–Morris models.

The pseudo-first-order model can be mathematically expressed by the equation [39]:

$$\frac{dq_t}{dt} = k_1(q_e - q_t) \quad (6)$$

where  $q_t$  ( $\text{mg}/\text{g}$ ) is the concentration of EX removed from the solution at time  $t$ ,  $t$  is the time (min),  $k_1$  is the rate constant of the pseudo-first-order model ( $1/\text{min}$ ), and  $q_e$  is the concentration of EX removed from the solution at equilibrium ( $\text{mg}/\text{g}$ ). By integrating Equation (6), its linear form is obtained as follows:

$$\ln q_t = \ln q_e + k_1 t \quad (7)$$

The pseudo-second-order model can be mathematically expressed by the equation [39]:

$$\frac{dq_t}{dt} = k_2(q_e - q_t)^2 \quad (8)$$

where  $k_2$  is the rate constant of the pseudo-second-order model ( $\text{g}/(\text{mg min})$ ). By integrating Equation (8), Equation (9) is obtained:

$$\frac{t}{q_t} = \frac{1}{kq_e^2} + \frac{1}{q_e} t \quad (9)$$

From the pseudo-second-order model, the initial rate of EX removal,  $h$  ( $\text{mg}/(\text{g min})$ ), can be determined under the condition that  $t \rightarrow 0$ :

$$h = kq_e^2 \quad (10)$$

Thus, Equation (10) becomes

$$\frac{t}{q_t} = \frac{1}{h} + \frac{1}{q_e} t \quad (11)$$

The values of  $q_e$  and  $k_2$  can be calculated from the slope and intercept of the straight line obtained from the dependence  $t/q_t = f(t)$ .

Boyd model can be expressed by Equation (12) [40]:

$$F = \frac{q_t}{q_e} = \left(1 - \frac{6}{\pi^2}\right) \exp -B_t \quad (12)$$

and

$$B_t = -0.4977 - \ln(1 - F) \quad (13)$$

where  $F$  is the fraction of EX adsorbed at any time,  $t$ ;  $q_e$  amount adsorbed at equilibrium (mg/g);  $q_t$  amount adsorbed at the time; and  $t$  and  $B_t$  are mathematical functions of  $F$ .

Weber–Morris intraparticle diffusion can be expressed by Equation (14) [39]:

$$q_t = I + k_d t^{1/2} \quad (14)$$

where  $k_d$  is the interparticle diffusion rate constant (mg/(g min<sup>1/2</sup>)),  $t$  is time (min), and  $I$  is the intercept on the y-axis.

### 3. Results and Discussion

#### 3.1. Chemical Analysis

The chemical composition of RWS is given in Table 1, while Table 2 presents the heavy metal content in the investigated RWS sample.

**Table 1.** The chemical composition of RWS [3].

wt. %	SiO <sub>2</sub>	Fe <sub>2</sub> O <sub>3</sub>	Al <sub>2</sub> O <sub>3</sub>	CaO	MgO	SO <sub>3</sub>	Na <sub>2</sub> O	K <sub>2</sub> O	P <sub>2</sub> O <sub>5</sub>	TiO <sub>2</sub>	LOI *
RWS	21.20	10.81	15.70	6.32	2.50	1.78	2.67	0.63	0.036	0.62	37.45

Note: \* LOI—the loss on ignition.

**Table 2.** The content of heavy metals in the RWS sample (in mg/kg).

Sample	Cr	Cu	Li	Mn	Ni	Pb	Zn	Cd	Sn	Sb	Ag
RWS	138	51	31	600	110	480	36	2.2	<5	160	5.4
MDK *	70	/	/	/	40	50	/	/	/	5.0	/

Note: \* The lower limit value for classifying waste as hazardous waste, according to the *Rulebook on Categories, Testing and Classification of Waste of the Republic of Serbia no. 56/2010, "Službeni glasnik"*.

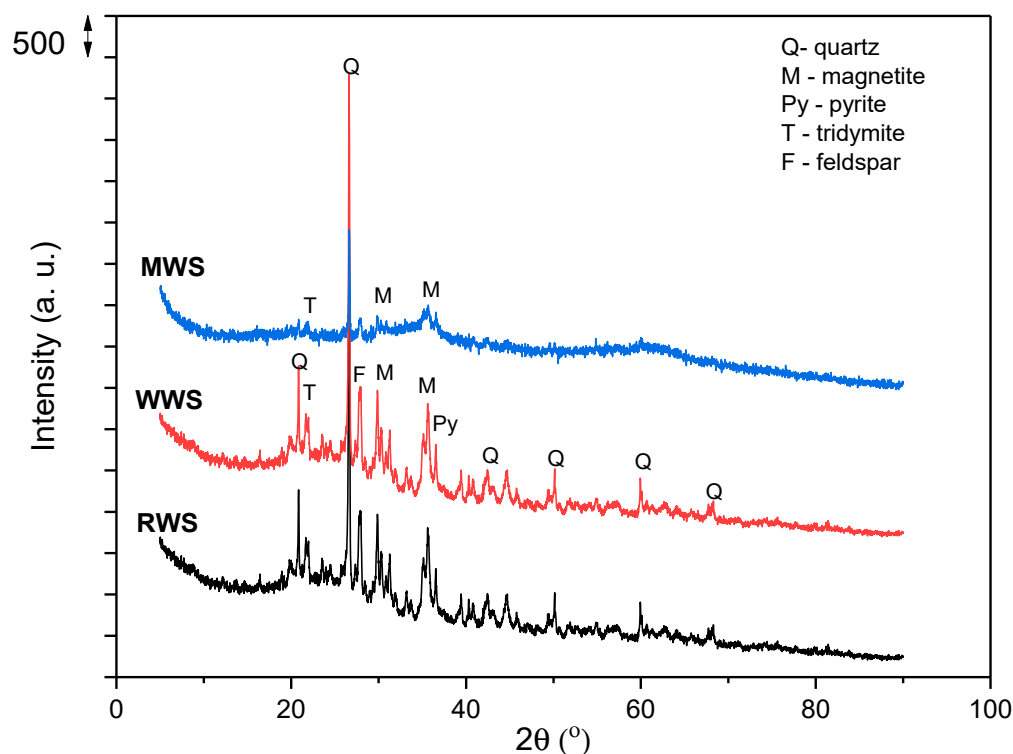
The results presented in Table 1 indicate that waste slag is rich in oxides of Si (21.20%), Fe (10.81%), and Al (15.70%), while other elements are less abundant. This sample is characterized by significant loss on ignition (37.45%), which means that the sample contains notable amounts of organic components. From the literature [41], it is known that the Si/Al ratio in the sample can be an indication of its hydrophobicity. Thus, the surface is hydrophilic if the Si/Al ratio is lower than 2, while the surface is hydrophobic if the Si/Al ratio is higher than 7. In the investigated waste slag sample, the Si/Al ratio is 1.35, which means its surface is hydrophilic.

Table 2 shows the content of the Cr, Ni, Pb, and Sb are significantly higher than the values allowed for the non-hazardous waste according to the *Rulebook on Categories, Testing and Classification of Waste of the Republic of Serbia no. 56/2010, "Službeni glasnik"*, and consequently, this material is classified as a hazardous waste.

#### 3.2. X-ray Diffraction Analysis

XRD analysis of the RWS sample (Figure 3), which is already published in our previous paper [3], showed that the sample in its crystal phase contains the following: quartz (SiO<sub>2</sub>), olivine ((Mg,Fe)<sub>2</sub>SiO<sub>4</sub>), magnetite ((Fe<sup>2+</sup>Fe<sup>3+</sup>)<sub>2</sub>O<sub>4</sub>), pyrite (FeS<sub>2</sub>), tridymite (SiO<sub>2</sub>), and feldspar ((Ca,Na,K)(Si,Al)<sub>4</sub>O<sub>8</sub>). The results are in agreement with those presented in Table 1, where a dominant presence has been established for Si, Al, Fe, and Ca. The high amount of Al but low amount of Na and K (elements present in the feldspar) indicate that this mineral is not present in significant amounts, as well as the fact that aluminum is not only present in the crystalline phase but is also present in the amorphous phase, perhaps, in the form of amorphous aluminum hydroxyphosphate sulfate. On the other hand, the low magnesium content indicates that olivine is also not present in significant quantities in the investigated sample and that iron is dominantly present in the form of magnetite or pyrite.





**Figure 3.** The XRD analyses of the RWS, WWS, and MWS.

The results of the XRD analyses of WWS and MWS are also presented in Figure 3.

The XRD diffractogram of the WWS sample shows good crystallinity. After a comparison of the results for WWS and RWS samples, it can be observed that the sample shows good crystallinity; therefore, no change in crystallinity occurs after washing.

In the presented diffractogram of the MWS sample, the crystal structure is significantly changed, and there is a decrease in the crystalline phase as well as a decrease in the intensity of the remaining quartz peaks. From the diffractogram of the MWS sample, only the peaks of quartz ( $2\theta \approx 26$ ) and low peaks of magnetite ( $2\theta \approx 35$ ) can be observed, while peaks of other phases disappeared due to structural transition from a crystalline to an amorphous phase. The amorphous part of the sample may contain hematite, aluminum silicates, and copper oxides in low amounts.

### 3.3. Infrared Spectroscopy with Fourier Transformation Analysis (FTIR)

In order to investigate functional groups present in the sample of raw, washed, and modified waste slag and to detect potential alterations in molecular structure due to washing and/or modification, the DRIFTS-FTIR (Diffuse Reflectance Infrared Fourier-Transform Spectroscopy) technique was applied. Recorded spectra of RWS, WWS, and MWS samples are presented in Figure 4.

In the DRIFT spectra of the RWS sample, spectral bands appear at  $3786$  and  $3697$   $\text{cm}^{-1}$ , originating from stretching the structural hydroxyl groups Al-OH and Si-OH vibrations [42,43]. Spectral bands at  $1042$ ,  $934$ ,  $804$ , and  $690$   $\text{cm}^{-1}$  represent vibrational symmetrical and asymmetrical stretching of Si-O and Si-O-Si bonds, which, according to their shape and position, correspond to quartz and tridymite, whose crystal phases are reconfirmed through the XRD analysis [43–45]. Spectral bands at  $1739$   $\text{cm}^{-1}$  originate from valence vibrations  $\text{-C=O}$  of carboxylic acids, aldehydes, and esters [46]. The analyzed slag is derived from lignite and, therefore, rich in aromatics, which is confirmed by the spectral band of aromatic stretching at  $1574$   $\text{cm}^{-1}$  [46]. In addition, the band at  $1494$   $\text{cm}^{-1}$  is of phenolic -OH stretching [47], while the spectral band at  $1288$   $\text{cm}^{-1}$  indicates stretching of the enol C-O [3]. The bands located at  $1109$  and  $546$   $\text{cm}^{-1}$  originate from the presence of magnetite [48]. Bands characteristic of olivine are not visible in the RWS spectrum due to overlapping with

other bands. All spectral bands visible in the spectrum of the RWS are also visible in the spectrum of the WWS sample and overlap, or a slight change in intensity and positions can be observed. Also, in the spectrum of WWS, an additional spectral band at  $1395\text{ cm}^{-1}$ , characteristic of pyrite [48], can be clearly observed. The same is true for the MWS sample, although the spectral band appears at  $1353\text{ cm}^{-1}$ . Since the modification was performed with copper, and the pH was adjusted to 10 during the modification, this band can be explained by the formation and presence of  $\text{Cu}(\text{OH})_2$  and  $\text{Cu-OH}$  vibration [49].

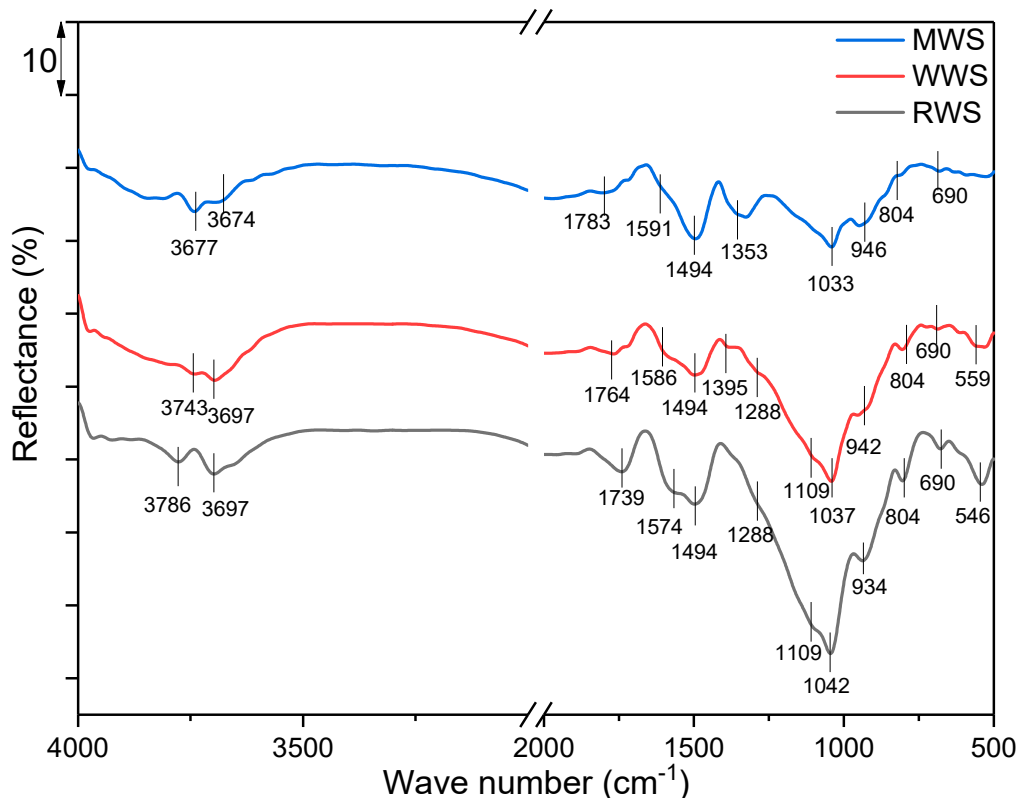


Figure 4. DRIFT spectra of RWS, WWS, and MWS samples.

### 3.4. Determination of Textural Properties

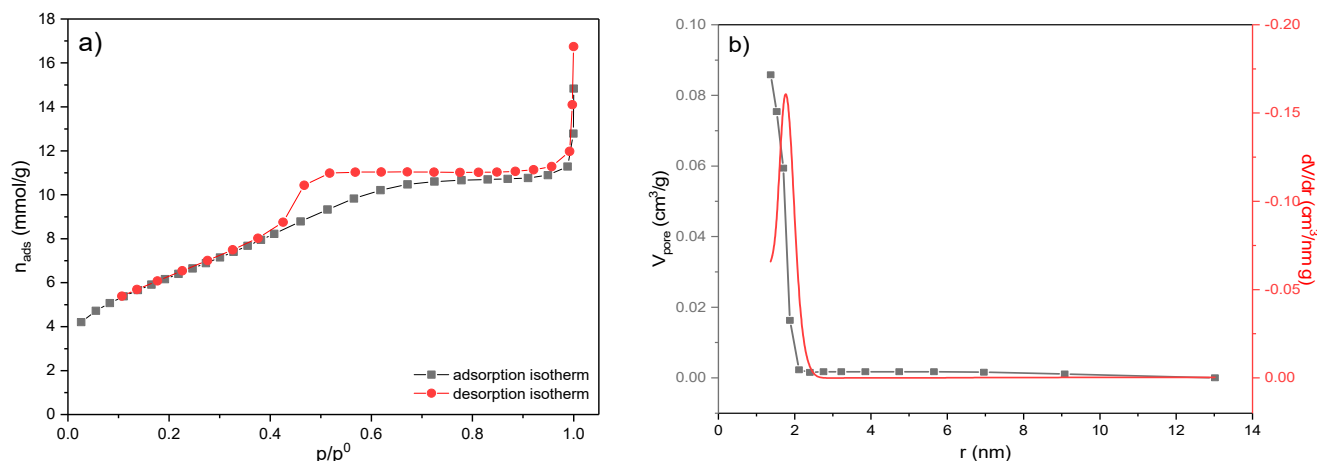
The surface area of the MWS sample was determined by BET analysis. Adsorption and desorption isotherms of  $\text{N}_2$  as a function of  $\text{N}_2$  relative pressure and at  $-196\text{ }^\circ\text{C}$  and corresponding pore size distribution curves are shown in Figure 5. At the same time, calculated textural parameters are presented in Table 3.

Table 3. Porous properties of the MWS sample.

Sample	$S_{\text{BET}}$ ( $\text{m}^2/\text{g}$ )	$V_{\text{total}}$ ( $\text{cm}^3/\text{g}$ )	$V_{\text{meso}}$ ( $\text{cm}^3/\text{g}$ )	$V_{\text{mic}}$ ( $\text{cm}^3/\text{g}$ )	$D_{\text{av}}$ (nm)	$D_{\text{max}}$ (nm)
MWS	170.46	0.07984	0.0795	0.00034	1.7699	1.7725 *

Note: \* The diameter of the pores that occupy the largest part of the volume.

According to the IUPAC classification [50], the isotherm is of type IV and has an H2 hysteresis loop associated with mesoporous materials (Figure 5a). The specific surface,  $S_{\text{BET}}$ , of the MWS sample is  $170.46\text{ m}^2/\text{g}$  and originates dominantly from the mesoporous structure of the sample.



**Figure 5.** The BET analysis of the MWS sample. (a) Nitrogen adsorption–desorption isotherms; (b) the pore size distribution curves determined by the Cranston and Inkley method.

The pore size distribution (PSD) of the MWS sample is presented in Figure 5b. It can be seen that the volume of mesopores ( $V_{meso}$ ) consists of pores between 1.4 and 2.2 nm, while the value of the pore diameter that occupies the largest part of the volume is 1.77 nm, indicating that the sample is completely mesoporous (according to IUPAC classification, micropores  $\leq 2$  nm, mesopores 2–50 nm, and macropores  $\geq 50$  nm), as a consequence of the particles' agglomeration.

It is well known that during modification, the morphological properties of surface material, such as specific surface area, pore volume, and pore size, change [51]. Bearing in mind that the specific surface of RWS was  $25 \text{ m}^2/\text{g}$  [3], which is  $\sim 7$  times lower than the value obtained for modified slag, it can be concluded that the modification of waste slug with copper and iron salts is a suitable choice for modification, as they significantly increase the adsorption surface area of the slag. In order to compare, the specific surface area of the WWS was also determined (results were not presented). The obtained results showed that the value of the specific surface area of the WWS sample did not change significantly compared to the RWS.

In addition, a larger surface area provides more active adsorption sites for the adsorption of xanthate molecules, and it is known that the increased porosity enhances the adsorption capacity of adsorbents [22]. Finally, the total pore volume of the MWS ( $0.08 \text{ cm}^3/\text{g}$ ) is approximately three times bigger than the total pore volume of the RWS ( $0.025 \text{ cm}^3/\text{g}$ ) [3].

### 3.5. Determination of the $pH_{pzc}$

The pH has a very important influence on the adsorption process. Namely, the pH affects the ionic form of the pollutant, the adsorbent surface charge, the potential chemical bonds or processes that can be realized on the surface of the material, etc. Thus, the determination of the PZC is very important since it gives information about the buffer properties of the material, the sensitivity of the material surface, the ionic strength in the solution, and also the charge on the surface under applied experimental conditions. This information is of particular importance for the explanation of the removal mechanism.

The PZC of the RWS, WWS, and MWS samples was determined for the  $pH_i$  from 2 to 12, and the obtained results are given in Figure 6.

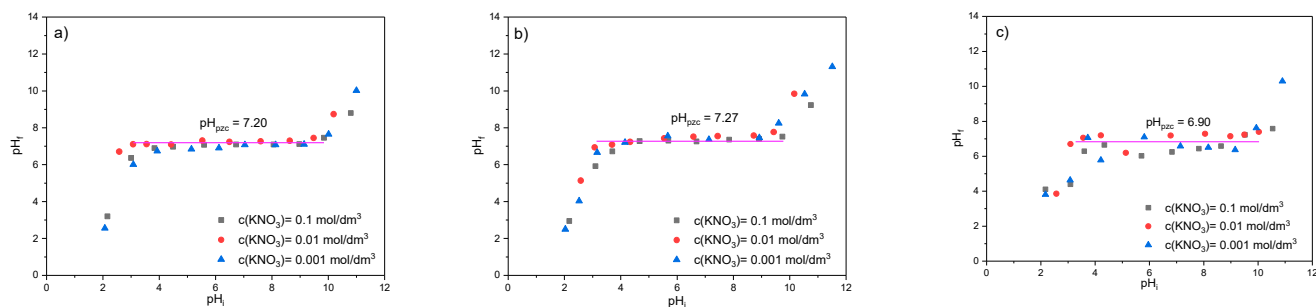


**Figure 6.** The dependence of final pH ( $\text{pH}_f$ ) on the initial pH ( $\text{pH}_i$ ) of three different ionic strengths for (a) RWS, (b) WWS, and (c) MWS.

As Figure 6a shows, for the RWS sample, when  $\text{pH}_i$  increases from 2 to 3, the final  $\text{pH}_f$  increases from 2 up to  $\sim 7$ . A further change of the initial pH from 3 to 10 does not cause a significant change in the final pH of the solution, while a further change of the initial pH results in an increase in the final pH up to  $\sim 11$ . From Figure 6a, it can also be seen that the same trend is obtained from all three ionic strengths. The plateau on the diagram marks the point of zero charge of the material and equals 7.20. Based on the literature [52,53], it can be concluded the surface is positively charged for  $\text{pH}_i$  up to 3, neutrally charged in the  $\text{pH}_i$  interval 3–10, and negatively charged for  $\text{pH}_i$  greater than 10. The good agreement of the points obtained for different ionic strengths, i.e., for different concentrations of  $\text{KNO}_3$ , indicates that the material has good stability, while the fairly long length of the plateau indicates that the RVS sample has very good buffering properties.

For WWS and MWS samples (Figure 6b,c), the same trends can be observed with the plateaus obtained in the initial pH range of 3–10. For these two samples, a slight change in the point of zero charge compared to the RWS was obtained, and it equaled 7.27 and 6.90, respectively. For the WWS sample, there was no significant dispersion of points, indicating that in addition to the unchanged buffer properties, the stability in comparison to the RWS was not changed either. However, in the case of the MWS sample, a certain degree of scattered points was observed, pointing out that modification reduced the stability of the material, depending on the ionic strength in the solution, but it still can be classified as satisfying.

### 3.6. Chemical Stability of EX

In order to define the optimal conditions for EX removal, as well as to determine its stability, i.e., to ensure the accuracy of the results, the stability of EX in the pH range of 2–12 was first examined. The obtained results are shown in Figure 7.

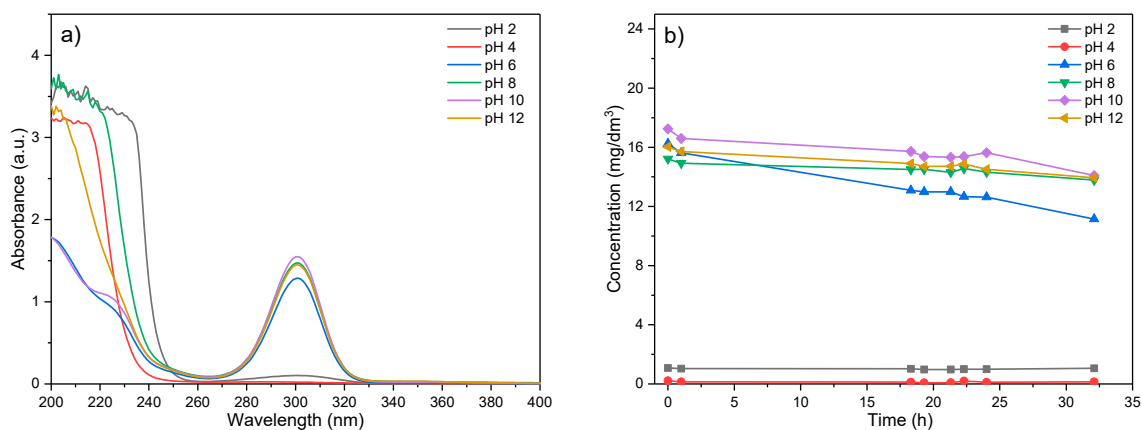


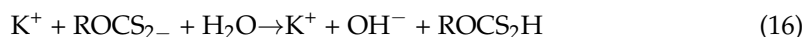
**Figure 7.** Determination of the chemical stability of EX in solution: (a) dependence of the intensity of the EX peaks as a function of the initial pH of the solution and (b) concentration of the EX as a function of time.

As presented in Figure 7a, in the spectrum of ethyl xanthate, two characteristic peaks were visible. The peak with the highest intensity at 300 nm originated from the presence of the ethyl xanthate anion ( $\text{EtOCS}_2^-$ ), while the peak at 206 nm is a consequence of the presence of the disulfide-carbide ( $\text{CS}_2$ ) [54,55].

In Figure 7b, the changes of EX anion concentrations as a function of time for different initial  $\text{pH}_i$  values are given. The characteristic curve of the EX anion decreases slightly over time for initial pHs higher than 8, indicating very low degradation and change of EX anion concentration in the solution. For pH values where the concentration of the EX anion decreases, an increase in the peak at 206 nm is noted, which might be explained by the formation of disulfide-carbide ( $\text{CS}_2$ ), a xanthate hydrolysis product. The chemical reaction of the ethyl xanthate degradation process could be presented by the following equation [56]:



According to the results in Figure 7, it could be noticed that in a very acidic environment, the degradation of EX occurs almost instantly during the dissolution because at the initial time of measurements, the degradation was 98.96% for  $\text{pH} = 2$ , while at  $\text{pH} = 4$ , the degradation takes several minutes, and it was 94.80%, which could be explained by the following reaction [54]:



In a slightly acidic and basic environment ( $6 \leq \text{pH} \leq 8$ ), the degradation of EX lasts for several hours, reaching a maximum value of 39.19% for  $\text{pH} = 6$  and 31.07% for  $\text{pH} = 8$  after 24 h.

The lowest degree of degradation of ethyl xanthate is observed at  $\text{pH} = 10$  or higher (<10%), and therefore, further experiments were performed at this  $\text{pH}_i$  value.

### 3.7. Initial Test of Ethyl Xanthate Anion Removal

An initial test for the removal of xanthate anions from the contaminated aqueous solutions on the RWS, WWS, and MWS samples was carried out, and the results are given in Figure 8.

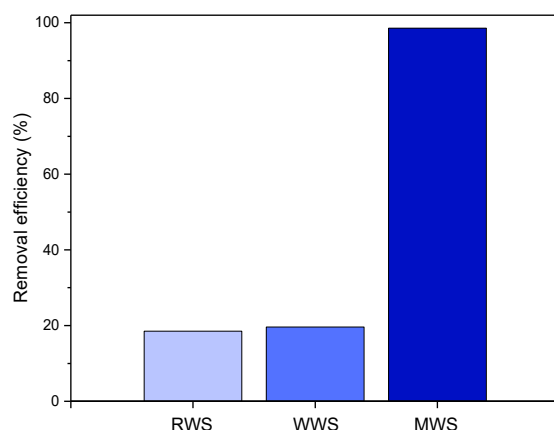


**Figure 8.** Results of  $20 \text{ mg/dm}^3$  xanthates removal by 10 mg RWS, WWS, and MWS slag C in  $50 \text{ cm}^3$  at  $\text{pH} 10$  and at  $25 \text{ }^\circ\text{C}$ .

As shown in Figure 8, the RWS and WWS samples showed a very low degree of EX anion removal (<20%). On the contrary, the removal efficiency for the MWS sample is significantly higher and equals about 99%. Based on these results, only the modified waste slag was used in further experiments. Considering such a significant difference, all other EX anions adsorption tests were performed only on the MWS sample.

### 3.8. Influence of the Initial $pH_i$ on the EX Anion Removal

The pH of the solution has a significant role in the adsorption process. Previous results presented in Figure 7 showed satisfactory stability of EX at  $pH > 8$  since only at these pH values is the EX in the form of anion ( $EtOCS_2^-$ ), whose removal is the subject of current research. For this reason, testing of the influence of pH was carried out in the pH range of 8–12, and the obtained results are shown in Figure 9.

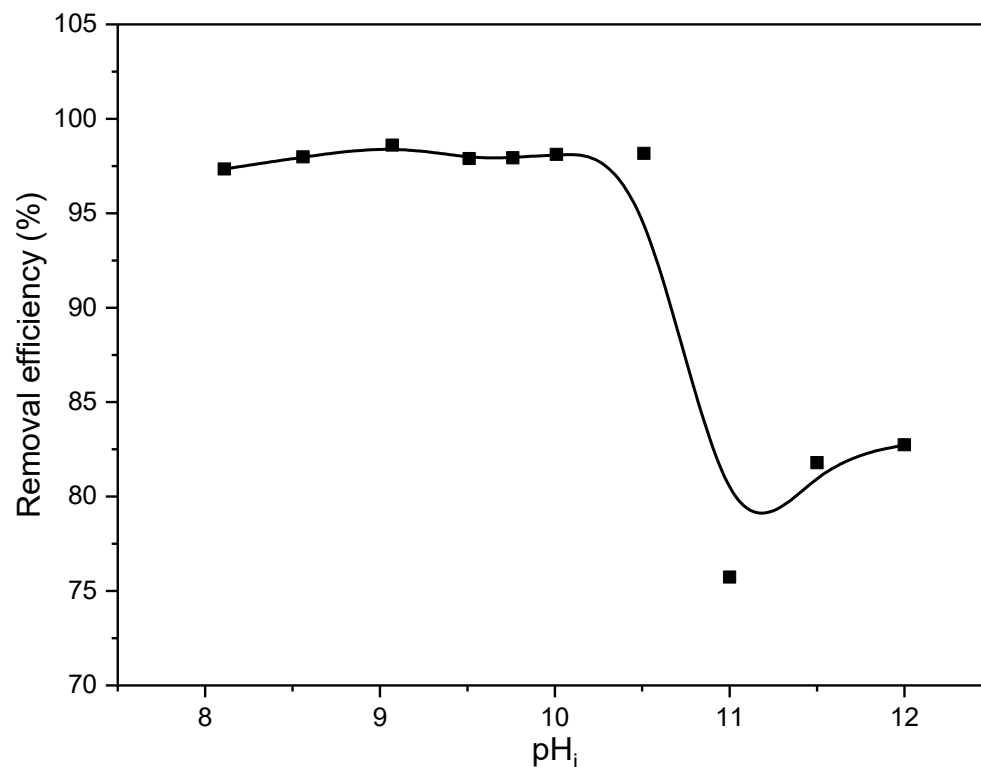


**Figure 9.** The removal efficiency of ethyl xanthate anions on the MWS as a function of  $pH_i$ .

According to the results, the removal efficiency did not change significantly in the pH interval 8–10.5 and was about 98.12%. At pH levels greater than 10.5, there is a decrease in efficiency to about 80%. This can be related and explained by the results of the point of zero charge. Namely, the results shown in Figure 6 showed that the surface of the MWS sample at  $pH_i$  up to 10 is electroneutral, while at  $pH_i$  higher than 10, it is negatively charged. Consequently, the decrease in removal efficiency of about 20% obtained for pH higher than 10 can be explained by the electrostatic repulsion of the negatively charged surface and the negatively charged xanthate  $EtOCS_2^-$  ion. However, it is important to note that despite this, the removal efficiency is still high (about 80%), which may be an indication that, in addition to the electrostatic forces, there are other mechanisms, which include the formation of the chemical bonds, involved in the removal of EX anions.

According to these results, and in line with other experiments, further analyses were conducted at pH 10. At this  $pH_i$  value, the EX anion is the most stable, and the surface of the waste slag is electrically neutral; hence, the highest efficiency could be expected.

### 3.9. Influence of Adsorbent Amount on the Removal of EX Anions

The investigation of the influence of the amount of the solid phase (MWS) on ethyl xanthate anion removal actually gives the answer related to the optimal solid/liquid phase ratio that would enable the most effective ethyl xanthate anions adsorption. The experiments were performed for the amount of the MWS up to  $10,000 \text{ mg/dm}^3$ , and the results are given in Figure 10.

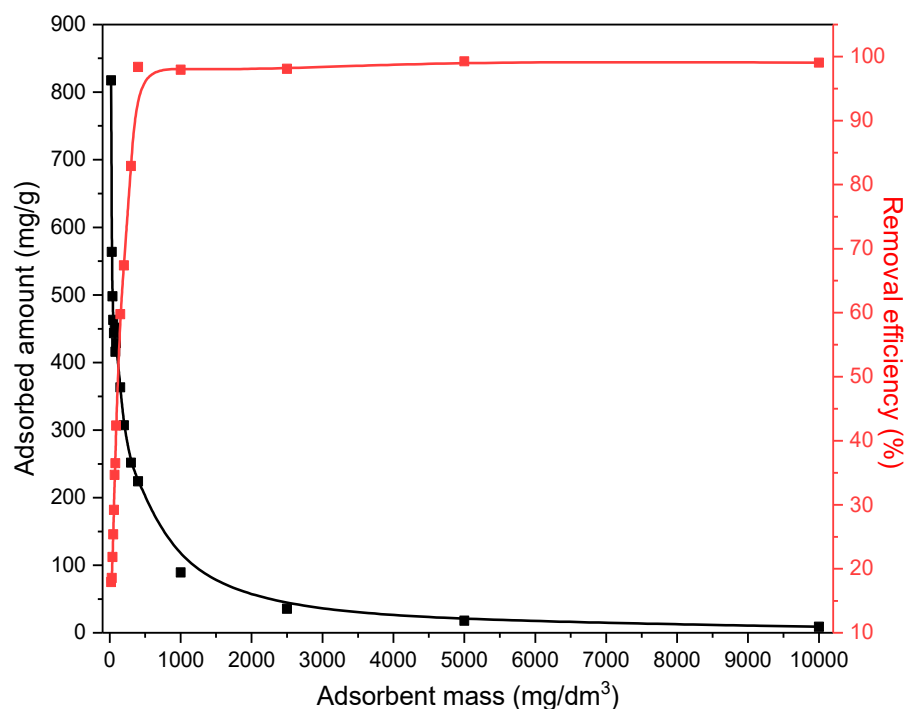


**Figure 10.** The effect of MWS amount on EX anion removal.

As shown in Figure 10, the percentage of EX anion removal (red curve) increases with the increase in the adsorbent mass. Such a trend is expected because increasing the adsorbent mass also increases the surface area available for the adsorption, resulting in a greater number of binding sites. From the presented results, it is obvious that the percentage of the EX anion removal increases exponentially and reaches a plateau for the mass of MWS of 400 mg/dm<sup>3</sup>. However, at the same time, the adsorbed amount of the EX anions expressed in the mg/g (black curve) showed a decreasing trend with the increase in the waste slag mass. In the literature [57,58], there are two explanations for this phenomenon. The first explanation is that the increase in the adsorbent amount could lead to the increasing possibility of collision between the adsorbent particles, which may cause their precipitation or coagulation and thereby reduce the number of binding sites. The second explanation for this trend is that increasing the mass of the solid phase (from 20 mg/dm<sup>3</sup> to 10,000 mg/dm<sup>3</sup>) is significantly greater than the increase in the adsorbed amount (20 mg/dm<sup>3</sup> of MWS adsorbed 16.35 mg/dm<sup>3</sup> of EX anions, while an increasing amount of the adsorbent 500 times (10,000 mg) causes an increase in the adsorption of EX by 5.5 times (90.2 mg/dm<sup>3</sup>) of the EX anions), leading to an apparent decrease in the EX anions adsorption capacity expressed in mg/g.

According to the presented results and their comparison with the explanations from the literature, it can be observed that the contact surface area between the solid and liquid phases, the adsorbent and the adsorbate, should not be increased indefinitely as it may produce the opposite effect. Therefore, careful determination of the ratio of the solid–liquid phase reaction is essential. During the experiments, all suspensions were constantly mixed, and no particle precipitation or coagulation was observed. Hence, the second-mentioned theory can be applied to explain the obtained results. According to this theory, the highest removal efficiency expressed in % is achieved with a maximum quantity of 10,000 mg/dm<sup>3</sup> of MWS. Although the results and explanations indicate that the most effective EX removal occurs at the maximum content of modified waste slag, a concentration of 200 mg/dm<sup>3</sup> (10 mg/ 50 cm<sup>3</sup>) was used for further experiments. This mass was chosen as the optimal ratio of the adsorption capacity in mg/g and the percentage of EX removal while ensuring that both values remain as high as possible. The intersection of

these two curves in Figure 10 is very close to the 200 mg/dm<sup>3</sup> of the MWS, so this amount was used in further investigations.

Table 4 presents the comparison of the adsorption capacity of the MWS sample with different adsorbents found in the literature. It can be clearly seen that MWS possesses a higher adsorption capacity than other adsorbents mentioned in published studies [20–23].

**Table 4.** Comparison of the adsorption capacities of various adsorbents found in literature and those obtained in this study.

Adsorbents	pH	Mass of Adsorbent (mg/dm <sup>3</sup> )	Initial Concentration (mg/dm <sup>3</sup> )	q <sub>max</sub> (mg/g)	Reference
AgNPs-clinoptilolite	9.70	200	20	99.0	[20]
Al-Be	12.2	7500	2000	264.0	[21]
Be-Cu-Fe <sub>2</sub> O <sub>4</sub>	9.2	4000	1000	235.0	[22]
Mn-Ce-Al <sub>2</sub> O <sub>3</sub>	7.22	500	100	197.4	[23]
MWS	9–10	200	100	307.1	This paper

### 3.10. Influence of EX Anions Concentration on the Removal Efficiency of the MWS

The initial concentration of the pollutant is one of the most important parameters affecting the adsorption efficiency. The rate of binding, as well as whether it will occur only on the surface or in the pores of the adsorbent, depends significantly on the initial concentration of the pollutant. Therefore, the experiments were carried out for initial EX anions concentrations in the range of 10–100 mg/dm<sup>3</sup> and for an adsorbent mass of 10 mg in 50 cm<sup>3</sup> solution at 25 °C. The obtained results are presented in Figure 11.

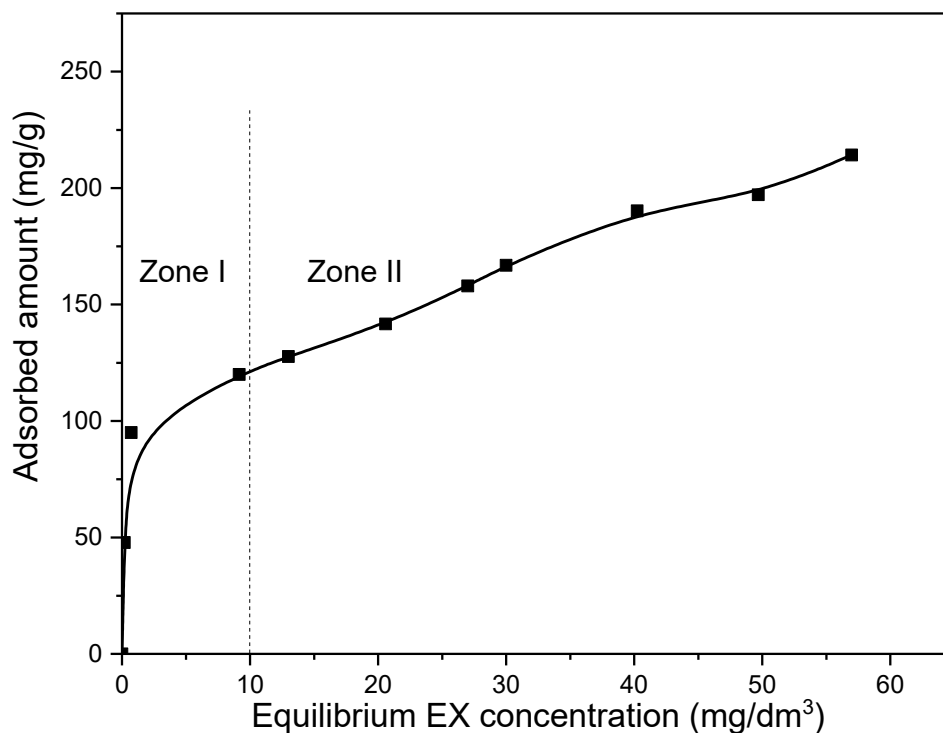


**Figure 11.** Influence of initial EX anions concentration on removal efficiency of the MWS.

As Figure 11 shows, when the initial concentration of the EX anions increased up to ~30 mg/dm<sup>3</sup> (equilibrium concentration 10 mg/dm<sup>3</sup>—Zone I), the adsorbed amount increased rapidly from zero up to ~120 mg/g (0–80%). A further increase in the initial concentration up to 100 mg/dm<sup>3</sup> (equilibrium concentration 57 mg/dm<sup>3</sup>—Zone II) also causes an increase in the adsorbed amount. However, for the highest initial concentration



(100 mg/dm<sup>3</sup>), a significantly slower trend was obtained, and the maximum adsorption was about 210 mg/g (42% adsorbed). It is important to note that there was no saturation of the MWS sample in the entire investigated range, so the dependence curve in the entire range showed an increasing trend. A rapid increase in the adsorbed amount with an increase in the initial concentration of EX anions in Zone I may be an indication that in that range of initial concentration the binding of EX anions most likely occurred on the surface at easily accessible sites by processes or mechanisms that take place quickly and, thus, do not include the formation of chemical bonds. After that, in Zone II, a slower increase in the adsorbed amount with the increase in initial concentration can be observed and indicates that the binding process takes place in hard-to-reach sites and/or by processes that take place more slowly and require the formation of chemical bonds. Moreover, not reaching saturation might indicate that adsorption does not take place on the surface in a monolayer.

To better describe and define the mechanism of EX anion adsorption on the MWS sample, three adsorption models (Langmuir, Freundlich, and Temkin) were used to fit the results. The linear fits of the applied isotherms are shown in Figure 12a–c and Table 5.

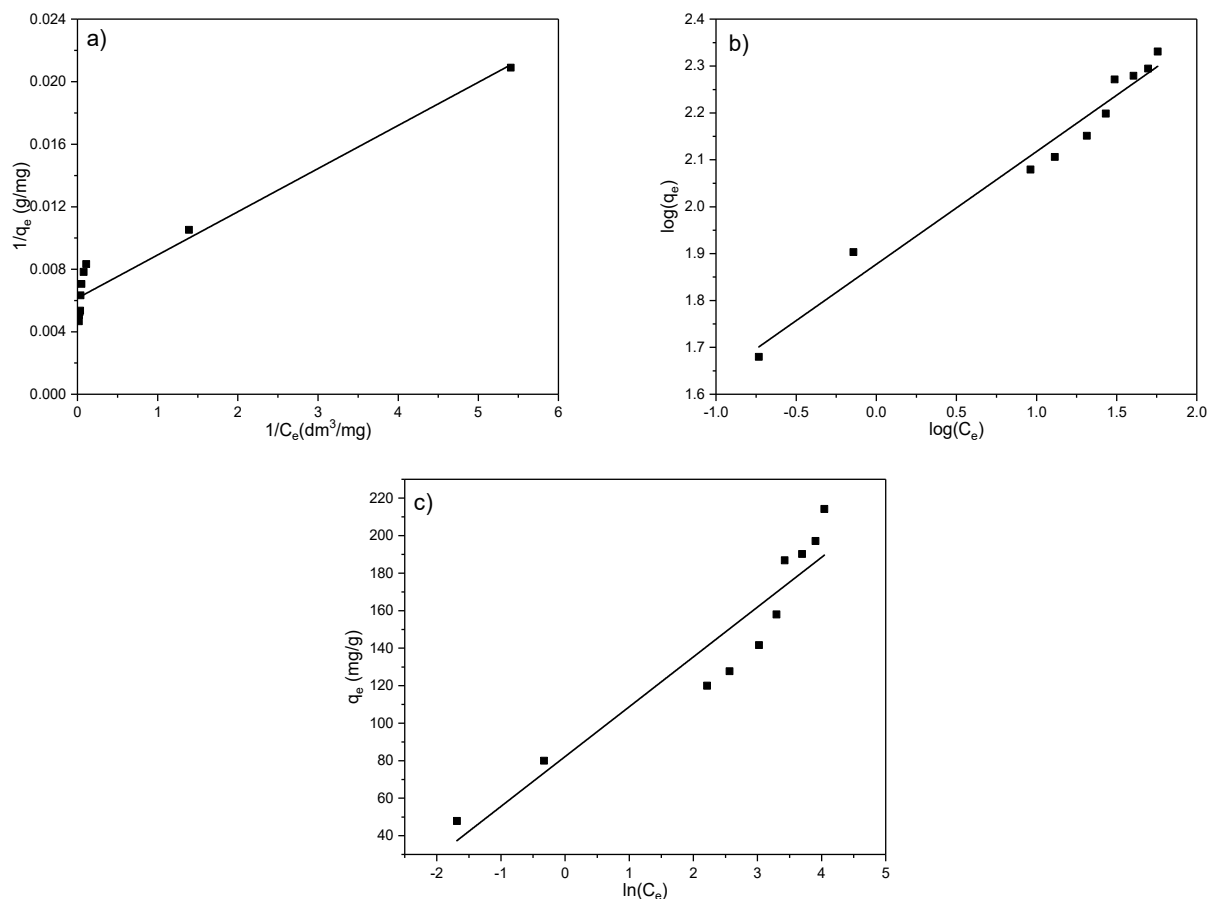


**Figure 12.** Linear fits of the adsorption isotherms for EX anion removal on the MWS. (a) Langmuir model; (b) Freundlich model; (c) Temkin model.

From the results presented in Figure 12 and Table 5, it can be seen that a satisfying correlation coefficient ( $R^2 = 0.94$ ) was obtained for the Langmuir and Freundlich models. However, although the correlation coefficient for the Langmuir model was found to be high (0.94), it can be noted that the maximum adsorbed amount obtained experimentally (213.89 mg/g) and the amount obtained by the model (162.60 mg/g) (Table 5) differ for 24%. The high value of  $R^2$  originates from the symmetrical deviation of the points from the fitted line; nevertheless, the significant difference between  $q_{\max, \text{theor}}$  and  $q_{\max, \text{exper}}$  indicates that the Langmuir model does not sufficiently describe the adsorption of EX anions on the MWS

sample. That means no monolayer is formed on the surface, which corresponds to the assumption based on the results presented in Figure 11.

**Table 5.** Adsorption isotherms parameters obtained from linear curves for EX adsorption.

Adsorption Isotherm	Adsorption Parameters	Value
Langmuir	$q_{\max, \text{theor}}$ (mg/g)	162.60
	$q_{\max, \text{exper}}$ (mg/g)	213.89
	$b$ (dm <sup>3</sup> /mg)	2.23
	$R^2$	0.94
Freundlich	$K_F$ (dm <sup>3</sup> /mg)	75.39
	$n$	4.17
	$1/n$	0.24
	$R^2$	0.97
	$\Delta G^0$ (kJ/mol)	−10.71
Temkin	$K_t$ (dm <sup>3</sup> /mg)	21.98
	$b$	93.26
	$R^2$	0.88

The Temkin isotherm model is based on the assumption that the heat of adsorption of all the molecules in a layer decreases linearly due to an increase in surface coverage of the adsorbent, i.e., it considers the effect of indirect adsorbate–adsorbent interaction on the adsorption process. The adsorption is characterized by a uniform distribution of binding energies up to its maximum. However, for the Temkin model, the  $R^2$  was significantly lower (0.88) compared to the Langmuir and Freundlich, so this model does not describe well the processes involved in the adsorption of EX anions on the MWS sample. Inapplicability of the Temkin model indicates that the decrease in heat of adsorption is logarithmic rather than linear, as implied in the Freundlich isotherm.

Thus, the only model that could be applied to the results of the removal of the EX anions by using the MWS sample is the Freundlich model ( $R^2 = 0.97$ ). The best agreement of the results with the Freundlich model confirms that the surface of the adsorbent is heterogeneous (which is, in general, characteristic of natural materials), the adsorption does not occur in a monolayer, and the binding of EX anions takes place in a complex manner [54]. The high value of the Freundlich constant,  $K_F$  (75.39 dm<sup>3</sup>/mg), confirms the high adsorption capacity of the MWS sample for EX anions. Further, the  $K_F$  value was used for the calculation of the change of the standard Gibbs free energy ( $\Delta G^0$ ) of the adsorption by using the equation:  $\Delta G^0 = -RT \ln(K_F \times 1000)$ , where  $R$  is the gas constant (8.314 J/(K mol)), and  $T$  is the temperature (298 K). Furthermore, the negative value of the  $\Delta G^0$  (−10.71 kJ/mol) in Table 5 is an indication of the feasibility of the process and the spontaneous nature of the adsorption. However, this result should be used with caution, given that there are disagreements in the literature regarding the application of this equation in practice [59–65].

The parameter  $n$  is a measure of the adsorption intensity, while the parameter  $1/n$  is a measure of the surface heterogeneity. So, for favorable adsorption,  $1/n$  is between 0 and 1, and for unfavorable adsorption,  $1/n$  is higher than 1, while if it is equal to 1, that indicates linear adsorption. If the  $1/n$  value is close to 0, the adsorption process is irreversible [64]. In this research, the  $1/n$  was 0.24, which, in addition to the negative value of the  $\Delta G^0$ , confirms the adsorption of the EX anions on the surface of the MWS sample as favorable [65].

During these experiments, the final pH<sub>f</sub> values at the end of reaction time for every initial concentration were also measured, and results are presented in Figure 13.

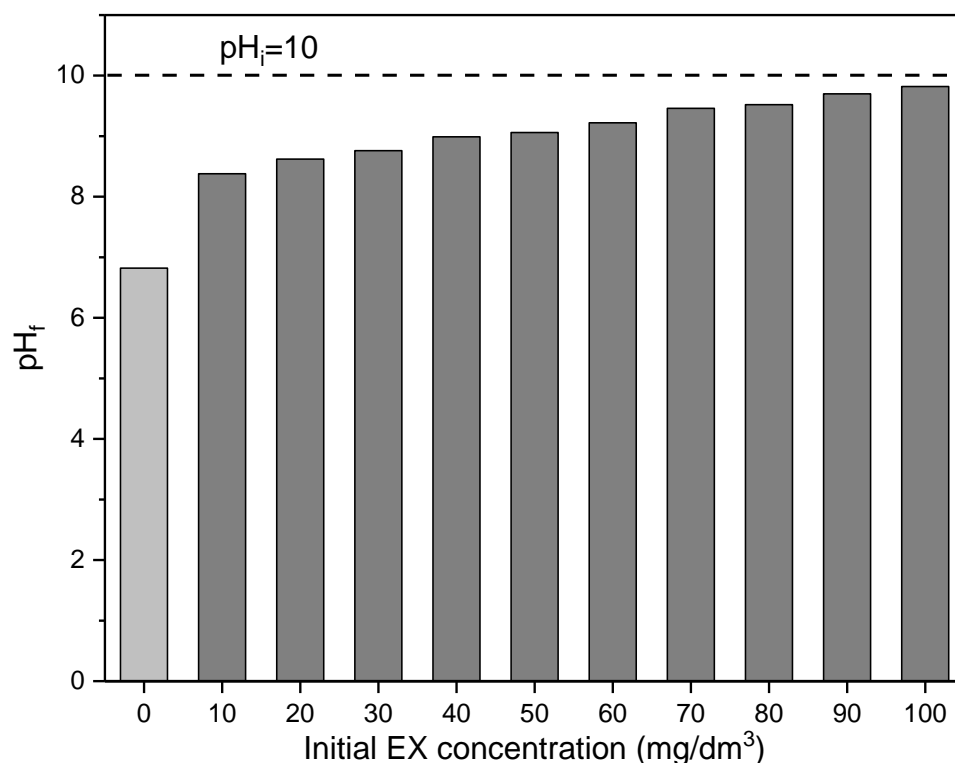


**Figure 13.** Dependence of the pH<sub>f</sub> of initial EX concentration. The dashed line is pH<sub>i</sub>.

As can be seen in Figure 13, after reaction time, the final pH decreased for each initial EX anions concentration in comparison with initial pH<sub>i</sub> = 10, although the values were higher compared to the pH of the solution without the presence of the EX anions (pH = 6.82). The largest decrease in pH was recorded for the lowest initial concentration (10 mg/dm<sup>3</sup>) of EX anions ( $\Delta\text{pH} = 1.64$ ), where 80% of EX anions was adsorbed, while the smallest decrease was observed for the highest initial concentration of EX anions (100 mg/dm<sup>3</sup>), where 42% EX anions were adsorbed. The final pH values were between the initial solution (pH<sub>i</sub> = 10) and the pH of the aqueous solvent suspension (pH = 6.82). The change in pH is proportional to the change in the initial concentration of EX anions and, consequently, cannot be considered for an explanation of the adsorption mechanism. Moreover, it is very important to emphasize that in all experiments, the pH value was in the range where EX is in the form of EtOCS<sup>2-</sup> anions (Figure 7). Also, for all these pHs, the surface of the MWS sample was electroneutral (Figure 6), indicating that electrostatic interactions did not affect the removal of EX anions.

### 3.11. Kinetic of EX Anion Removal

The kinetics of the adsorption process is particularly important for aspects of practical applications of the adsorbent, where shorter contact time is desirable. On the other hand, kinetic results give information about the adsorption mechanisms. During the investigation of the kinetics of adsorption, it is also important to choose the appropriate pollutant concentration, which should not be too high or too low, because the obtained results in that case can lead to wrong conclusions. Thus, it is best to work in the medium concentration range. In this research, the kinetics were investigated for the initial EX concentration of 50 mg/dm<sup>3</sup>, and results are presented in Figure 14.

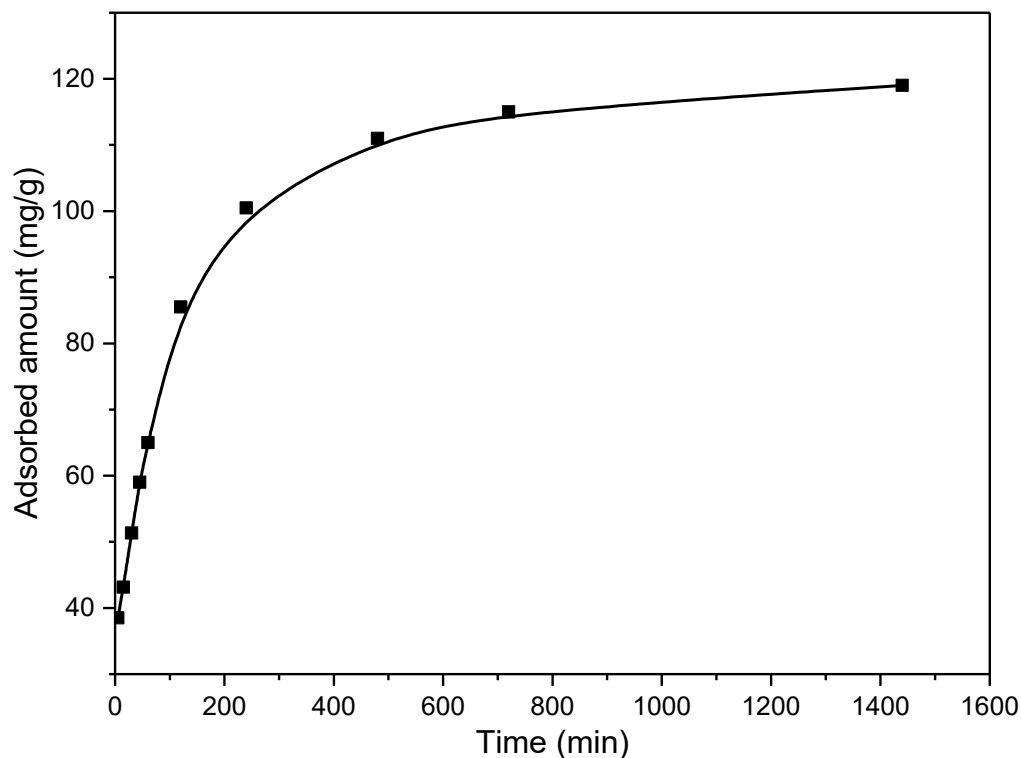


**Figure 14.** Influence of contact time on the EX removal by the MWS sample.

As it is presented in Figure 14, the adsorption of EX was rapid in the first ~240 min, achieving a capacity of ~100 mg/g. Afterward, a slowing down of the adsorption rate can be observed, reaching adsorption equilibrium at ~approximately 700 min, with a maximum capacity of 119.2 mg/g. Namely, at the beginning of the process, there is a significant number of easily available sites for EX anion removal. However, with time, the number of these sites decreases, and the repulsion forces of the adsorbed molecules occur, which causes inhibition of the adsorption process.

Evaluation of the overall adsorption rate and adsorbent performance through the chemical reaction-based and diffusion-based kinetic models is of great importance for understanding the adsorption mass transfer mechanisms, the resistances to the mass transfer, as well as for the proper design of the adsorption system. Many researchers reported the internal diffusion of the adsorbate in the pores of the adsorbents as the slowest adsorption step, while some findings pointed to the adsorption on active sites as the slowest step [66–71]. Therefore, the pseudo-first-order (PFO) and pseudo-second-order (PSO) models, as well as Boyd and Weber–Morris models, were applied on experimentally obtained adsorption results for an initial EX concentration of 50 mg/dm<sup>3</sup> and temperature of 25 °C. The fitting of the experimentally obtained results and parameters calculated by application of the above-mentioned models are given in Figure 15 and in Table 6

From Figure 15a and the results presented in Table 6, it can be seen that the PFO model does not apply to the obtained experimental results, especially after approximately 50 min from the beginning of the adsorption. This follows the data available in the literature, where the PFO model fits better in the case of higher initial pollutant concentrations and, consequently, better describes the initial adsorption phase. It is based on the assumption that adsorbate binds to one active site with a rate of occupation proportional to the number of adsorbent available sites [68,69,71]. Despite high correlation coefficients ( $R^2 = 0.99$ ), noticeable differences in experimentally obtained capacity ( $q_{e,exp}$ ) and that calculated by the model ( $q_{e,model}$ ) point to the unsuitability of the pseudo-first-order model in the description of EX adsorption on the MWS.

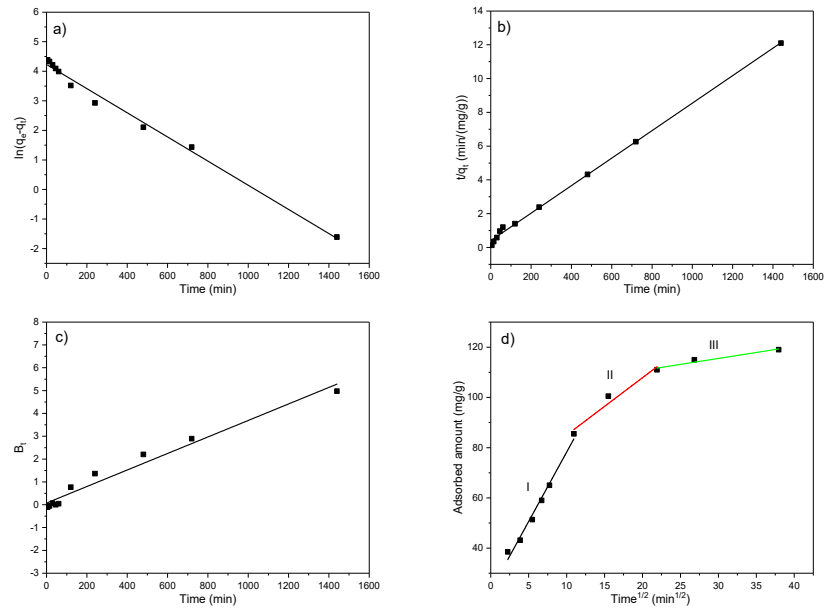


**Figure 15.** Fitting of the obtained results according to the (a) PFO model, (b) PSO model, (c) Boyd model, and (d) Weber–Morris model for initial EX concentration of 50 mg/dm<sup>3</sup> and temperature of 25 °C.

**Table 6.** Parameters of the kinetic models.

Kinetic Parameters for EX Initial Concentration of 50 mg/dm <sup>3</sup>	
Pseudo-First-Order	
$q_{e,model}$ , mg/g	11.49
$q_{e,exp}$ , mg/g	119.2
$k_1$ , 1/min	$4.09 \times 10^{-3}$
$R^2$	0.99
Pseudo-Second-Order	
$q_{e,model}$ , mg/g	121.8
$q_{e,exp}$ , mg/g	119.2
$k_2$ , g/(mg min)	$2.02 \times 10^{-4}$
$h$ , mg/(g min)	3.00
$R^2$	0.99
Boyd	
$R^2$	0.97
Weber–Morris Model	
Zone I	
$k_d$ , mg/(g min <sup>1/2</sup> )	5.51
I	23.09
$R^2$	0.98
Zone II	
$k_d$ , mg/(g min <sup>1/2</sup> )	2.28
I	62.224
$R^2$	0.92
Zone III	
$k_d$ , mg/(g min <sup>1/2</sup> )	0.48
I	101.27
$R^2$	0.91

Conversely, the PSO model (Figure 15b) based on chemisorption is better fitted to the experimental data than the PFO model, with high  $R^2 = 0.99$ , as well as very close values of  $q_{e,exp}$  and  $q_{e,model}$  (Table 6), indicating that adsorption of EX on the MWS better follows the second-order rate. Namely, the PSO model assumes the binding of adsorbate to two active sites and better describes kinetics at lower initial pollutant concentrations. Consequently, it better describes the final phase of the adsorption process. Moreover, it also better describes the adsorption on modified materials since they are richer in active sites, compared to native (raw), which is why the kinetic is most affected by the third controlling step, i.e., adsorption on available active sites [70,71].

The Boyd ( $R^2 = 0.97$ ) and Weber–Morris ( $R^2 = 0.91$ – $0.98$ ) intraparticle diffusion-reaction models, which represent the internal mass transfer processes, yielded lower correlation coefficients compared to the PSO model. In Figure 15c, the obtained straight line did not pass through the origin (0, 0), meaning that intraparticle diffusion is not the sole rate-limiting step in the adsorption process [68,71]. Regarding the Weber–Morris model, since the plot of  $q_t$  vs.  $t^{1/2}$  in Figure 15d as a straight line did not pass through the origin ( $I \neq 0$ ), the adsorption is controlled by multiple processes, and intraparticle diffusion can simultaneously play an important role in the adsorption kinetics together with film diffusion, i.e., the external mass transfer [71–74]. Moreover, in Figure 15d, the multilinearity, i.e., the three linear sections, can be observed pointing to multiple mechanisms in controlling the adsorption process of EX onto the MWS. The first steeper linear segment (Zone I) includes the adsorption time up to ~120 min and represents EX binding onto the available active sites at the outer surface of the MWS, i.e., external diffusion. The second linear segment (Zone II) in Figure 15d, which includes the adsorption time ~120–480 min represents binding to the available sites in macropores and micropores of the MWS, i.e., the intra-particle diffusion, while the third linear segment (Zone III) from ~480 min to 1440 min represents the final equilibrium stage where the intraparticle diffusion becomes slow due to the decrease in pollutant concentration in the liquid phase over time. Similar findings were reported in the literature [68,74,75]. Namely, the increased concentration of adsorbate increases the diffusion driving force and, consequently, the diffusion rate. Thus, the intraparticle diffusion rate constant  $k_d$  had the highest value in Zone I and decreased up to the equilibrium (Zone III), meaning that a higher amount of adsorbate diffused into the adsorbent pores before being adsorbed [76]. On the contrary, the intercept on the y-axis,  $I$ , which represents the thickness of the boundary layer, increased from the beginning of the adsorption to the equilibrium. Namely, the higher pollutant concentration in the solution at the beginning of the adsorption ensured a better driving force for the external mass transfer process and, thus, a lower thickness of the boundary layer.

#### 4. Conclusions

From the results presented in this paper, it can be concluded that by applying adequate modification procedure by  $\text{Cu}(\text{NO}_3)_2$  and  $\text{Fe}(\text{NO}_3)_3$ , hazardous waste slag generated in the combustion process of lignite as a by-product could be transformed into efficient adsorbent for ethyl xanthate anions from contaminated aqueous solutions.

Detailed characterization showed that waste slag presents a potentially hazardous material with complex mineral and structural properties with the dominant presence of quartz, olivine, magnetite, pyrite, tridymite, and feldspar, which do not tend to significantly change after modification with the mentioned nitrates. Good buffer properties and pH stability can also be confirmed. However, significant improvement of textural properties occurred due to modification since the increase in the specific surface area from 25 for RWS to  $170 \text{ m}^2/\text{g}$  for the MWS sample was recorded. The point of zero charge also remains similar after modification (7.20 for RWS and 6.80 for MWS), while the surface charge of both was neutral for  $\text{pH}_i$  values between 3 and 10.

The adsorption experiments conducted at  $25^\circ\text{C}$  show that the optimal conditions, providing the highest percentage of ethyl xanthate anion removal from contaminated

aqueous solution, are a solid–liquid ratio of 10 mg/50 cm<sup>3</sup>, pH<sub>i</sub> = 10, and a reaction time of t<sub>max</sub> 700 min.

The results of the investigation of initial ethyl xanthate anions concentration influence the removal efficiency of the MWS, while the best fit of the Freundlich adsorption model confirms a complex but favorable adsorption mechanism, which does not occur in a monolayer. The best fit of the kinetic results is obtained according to the pseudo-second-order model, which suggests that chemisorption is included in ethyl xanthate anion removal by a complex mechanism. The good agreement of kinetic results with the Boyd and Weber–Morris model confirms that, besides chemisorption, which is present on the surface, a high amount of adsorbate diffuses into the adsorbent pores and cavities. Finally, successful utilization of waste slag could contribute to establishing innovative, cost-effective water treatment methods and better solid waste management in the industry sector, where the slag is widely present as a concerning waste stream.

**Author Contributions:** Conceptualization, M.K.; investigation, M.K., A.V., J.G., M.S., K.N. and N.N.; data curation, M.K. and I.N.; writing—original draft preparation, M.K., J.G. and A.V.; writing—review and editing, M.K., M.S., J.G. and I.N. All authors have read and agreed to the published version of the manuscript.

**Funding:** This research received no external funding.

**Data Availability Statement:** All data used for this study are contained within text.

**Acknowledgments:** These investigations were supported by the Ministry of Science, Technological Development and Innovation of the Republic of Serbia (contract numbers 451-03-66/2024-03/200017) through the realization of research themes 1702403 and 1702405.

**Conflicts of Interest:** The authors declare no conflicts of interest.

## References

- Korhonen, J.; Honkasalo, A.; Seppälä, J. Circular Economy: The Concept and its Limitations. *Ecol. Econ.* **2017**, *143*, 37–46. [[CrossRef](#)]
- Lacy, P.; Rutqvist, J. *Waste to Wealth: The Circular Economy Advantage*; Palgrave Macmillan: London, UK, 2015. [[CrossRef](#)]
- Nedeljković, A.; Stojmenović, M.; Gulicovski, J.; Ristić, N.; Milićević, S.; Krstić, J.; Kragović, M. Waste Slag from Heating Plants as a Partial Replacement for Cement in Mortar and Concrete Production. Part I—Physical–Chemical and Physical–Mechanical Characterization of Slag. *Minerals* **2020**, *10*, 992. [[CrossRef](#)]
- Gacal, F. *Lignite Coal—Health Effects and Recommendations from the Health Sector*; HEAL-Health and Environmental Alliance: Brussels, Belgium, 2018. [[CrossRef](#)]
- Životić, M.M.; Stojiljković, D.D.; Jovović, A.M.; Čudić, V.V. Mogućnost korišćenja pepela i šljake sa deponije termoelektrane “Nikola Tesla” kao otpada sa upotrebom vrednošću. *Hem. Ind.* **2012**, *66*, 403–412. [[CrossRef](#)]
- Kragović, M.; Ristić, N.; Gulicovski, J.; Nedeljković, A.; Pašalić, S.; Ristović, I.; Stojmenović, M. Application of Lignite Combustion Waste Slag Generated in Heating Plants as a Partial Replacement for Cement. Part II: Physical–Mechanical and Physical–Chemical Characterization of Mortar and Concrete. *Minerals* **2021**, *11*, 925. [[CrossRef](#)]
- Ma, M.; Wang, T.; Ke, X.; Liu, Y.; Song, Y.; Shang, X.; Han, Q. A novel slag composite for the adsorption of heavy metals: Preparation, characterization and mechanisms. *Environ. Res.* **2022**, *216*, 114442. [[CrossRef](#)] [[PubMed](#)]
- Hashim, Z.H.; Kuwahara, Y.; Hanaki, A.; Mohamed, A.R.; Yamashita, H. Synthesis of a CaO-Fe<sub>2</sub>O<sub>3</sub>-SiO<sub>2</sub> composite from a dephosphorization slag for adsorption of CO<sub>2</sub>. *Catal. Today* **2023**, *410*, 264–272. [[CrossRef](#)]
- Wills, B.A.; Finch, J. *Will’s Mineral Processing Technology: An Introduction to the Practical Aspects of Ore Treatment and Mineral Recovery*, 8th ed.; Elsevier Science Technology Books: Cambridge, MA, USA, 2016; ISBN 9780080970547.
- Byrne, K.M.; Monsefi, N.; Dawson, J.C.; Degasperi, A.; Bukowski-Wills, J.C.; Volinsky, N.; Kholodenko, B.N. Bistability in the Rac1, PAK, and RhoA signaling network drives actin cytoskeleton dynamics and cell motility switches. *Cell Syst.* **2016**, *2*, 38–48. [[CrossRef](#)] [[PubMed](#)]
- Aitio, A.; Kiilunen, M.; Santonen, T.; Nordberg, M. Gold and gold mining. In *Handbook on the Toxicology of Metals*; Academic press: Cambridge, MA, USA, 2022; Volume 2, pp. 817–843. [[CrossRef](#)]
- Bulatovic, S.M. Flotation of sulfide ores. In *Handbook of Flotation Reagents: Chemistry, Theory and Practice*; Elsevier Science & Technology Books: Cambridge, MA, USA, 2007; Volume 1, ISBN 0444530290.
- Harris, G.H. Xanthates. In *Reagents in Mineral Technology*; Routledge: Oxfordshire, England, UK, 2018; Volume 27, pp. 371–383.
- Boeing, D. Aquatic toxicity and environmental fate of xanthates. *Min. Eng.* **1998**, *50*, 65–68.
- Xu, Y.; Lay, J.P.; Korte, F. Fate and effects of xanthates in laboratory freshwater systems. *Bull. Environ. Contam. Toxicol.* **1988**, *41*, 5. [[CrossRef](#)]

16. Bach, L.; Nørregaard, R.D.; Hansen, V.; Gustavson, K. *Review on Environmental Risk Assessment of Mining Chemicals Used for Mineral*; Scientific Report; Aarhus University: Aarhus, Denmark, 2016; ISBN 978-87-7156-233-0.
17. Lin, H.; Qin, K.; Dong, Y.; Li, B. A newly-constructed bifunctional bacterial consortium for removing butyl xanthate and cadmium simultaneously from mineral processing wastewater: Experimental evaluation, degradation and biomineralization. *J. Environ. Manag.* **2022**, *316*, 115304. [[CrossRef](#)]
18. Jiang, M.; Zhang, M.; Wang, L.; Fei, Y.; Wang, S.; Núñez-Delgado, A.; Bokhari, A.; Race, M.; Khataee, A.; Klemeš, J.J.; et al. Photocatalytic degradation of xanthate in flotation plant tailings by TiO<sub>2</sub>/graphene nanocomposites. *Chem. Eng. J.* **2022**, *431*, 134104. [[CrossRef](#)]
19. Zhang, M.; Han, N.; Fei, Y.; Liu, J.; Xing, L.; Núñez-Delgado, A.; Jiang, M.; Liu, S. TiO<sub>2</sub>/g-C<sub>3</sub>N<sub>4</sub> photocatalyst for the purification of potassium butyl xanthate in mineral processing wastewater. *J. Environ. Manag.* **2021**, *297*, 113311. [[CrossRef](#)] [[PubMed](#)]
20. Panayotova, M.; Mintcheva, N.; Gicheva, G.; Djerahov, L.; Panayotov, V.; Ivanov, B. Xanthate removal from wastewater by using silver nanoparticles-zeolite composite. *Ecol. Saf.* **2019**, *13*, 58–67.
21. Rezaei, R.; Massinaei, M.; Moghaddam, A.Z. Removal of the residual xanthate from flotation plant tailings using modified bentonite. *Miner. Eng.* **2018**, *119*, 1–10. [[CrossRef](#)]
22. Amrollahi, A.; Massinaei, M.; Moghaddam, A.Z. Removal of the residual xanthate from flotation plant tailings using bentonite modified by magnetic nano-particles. *Miner. Eng.* **2019**, *134*, 142–155. [[CrossRef](#)]
23. Yaping, Z.; Chonghu, W.; Zhengzhong, L.; Jinmei, L. Catalytic ozonation of mineral processing wastewater containing Butyl Xanthate. In Proceedings of the International Conference on Computer Distributed Control and Intelligent Environmental Monitoring, Changsha, China, 19–20 February 2011.
24. Vidyashankar, S.; Ravishankar, G.A. Algae-based bioremediation: Bioproducts and biofuels for biobusiness. In *Bioremediation and Bioeconomy*; Elsevier: Amsterdam, The Netherlands, 2016; pp. 457–493. [[CrossRef](#)]
25. Terzić, A.; Pavlović, L.J.; Radojević, Z.; Pavlović, V.; Mitić, V. Novel Utilization of Fly Ash for High-temperature Mortars: Phase Composition, Microstructure and Performance Correlation. *Int. J. Appl. Ceram. Tec.* **2015**, *12*, 133–146. [[CrossRef](#)]
26. Rigaku. *PDXL Integrated X-ray Powder Diffraction Software*; Rigaku: Tokyo, Japan, 2011.
27. American Mineralogist Crystal Data Structure Base (AMCDSB). Available online: <http://rruff.geo.arizona.edu/AMS/amcsd.phpS> (accessed on 23 May 2023).
28. Gregg, S.J.; Sing, K.S.W. *Adsorption, Surface Area and Porosity*, 2nd ed.; Academic Press: London, UK, 1982; pp. 35–120.
29. Cranston, R.W.T.; Inkley, F.A. *The Determination of Pore Structures from Nitrogen Adsorption Isotherms in Advances in Catalysis*; Academic Press: London, UK, 1957; Volume 9, pp. 143–154.
30. Kaneko, K.; Ishii, C.; Ruike, M. Origin of superhigh surface area and microcrystalline graphitic structures of activated carbons. *Carbon* **1992**, *30*, 1075–1088. [[CrossRef](#)]
31. Kruk, M.; Jaroniec, M.; Gadkaree, K.P. Nitrogen adsorption studies of novel synthetic active carbons. *J. Colloid. Interface Sci.* **1997**, *192*, 250–256. [[CrossRef](#)] [[PubMed](#)]
32. Gulicovski, J.J.; Čerović, L.S.; Milonjić, S.K. Point of Zero Charge and Isoelectric Point of Alumina. *Mater. Manuf. Process.* **2008**, *23*, 615–619. [[CrossRef](#)]
33. Milonjić, K.S.; Ruvarac, A.; Šušić, M. The heat of immersion of natural magnetite in aqueous solutions. *Thermochim. Acta* **1975**, *11*, 261–266. [[CrossRef](#)]
34. Krishni, R.R.; Foo, K.Y.; Hameed, B.H. Adsorption of cationic dye using a low-cost biowaste adsorbent: Equilibrium, kinetic, and thermodynamic study. *Desal. Water Treat.* **2014**, *52*, 6088–6095. [[CrossRef](#)]
35. Chen, L.; Huan, Z.; Huan, L.; Liu, B.; Wang, G.; Yu, S. Characterization of Co (II) removal from aqueous solution using bentonite/iron oxide magnetic composites. *J. Radioanal. Nucl. Chem.* **2011**, *290*, 675–684. [[CrossRef](#)]
36. Freundlich, H.M.F. Over the adsorption in solution. *J. Phys. Chem.* **1906**, *57*, 385–471. [[CrossRef](#)]
37. Namal, P.; Lim, L.B.; Dahri, M.K.; Tennakoon, D.T. Dragon Fruit Skin as a Potential Low-cost Biosorbent for Removal of Manganese (II) Ions. *J. Appl. Sci. Environ. Sanit.* **2013**, *8*, 178–188.
38. Temkin, M.; Pyzhev, V. Kinetics of Ammonia Synthesis on Promoted Iron Catalysts. *Acta Physicochim. URSS* **1940**, *12*, 327–356.
39. Tan, I.A.W.; Hameed, B.H. Adsorption Isotherms, Kinetics, thermodynamics and Desorption of Activated Carbon Derived from Oil palm Empty Fruit Bunch. *J. Appl. Sci.* **2010**, *10*, 2565–2571. [[CrossRef](#)]
40. Campos, N.F.; Barbosa, C.M.; Rodríguez-Díaz, J.M.; Duarte, M.M. Removal of naphthenic acids using activated charcoal: Kinetic and equilibrium studies. *Adsorpt. Sci. Technol.* **2018**, *36*, 1405–1421. [[CrossRef](#)]
41. Wang, C.; Leng, S.; Guo, H.; Yu, J.; Li, W.; Cao, L.; Huang, J. Quantitative arrangement of Si/Al ratio of natural zeolite using acid treatment. *Appl. Surf. Sci.* **2019**, *498*, 143874. [[CrossRef](#)]
42. Patel, H.A.; Somani, S.R.; Bajaj, C.H.; Jasra, V.R. Nanoclays for polymer nanocomposites, paints, inks, greases and cosmetics formulations, drug delivery vehicle and wastewater treatment. *Bull. Mater. Sci.* **2006**, *29*, 133–145. [[CrossRef](#)]
43. Database of ATR-FT-IR Spectra of Various Materials. Available online: <https://spectra.chem.ut.ee/paint/fillers/quartz/> (accessed on 23 May 2023).
44. Correcher, V.; Garcia-Guinea, J.; Bustillo, A.M.; Garcia, R. Study of the thermoluminescence emission of a natural  $\alpha$ -cristobalite. *Radiat. Eff. Defect. S.* **2009**, *164*, 59–67. [[CrossRef](#)]



45. Bosch-Reig, F.; Gimeno-Adelantado, J.V.; Bosch-Mossi, F.; Doménech-Carbó, A. Quantification of minerals from ATR-FTIR spectra with spectral interferences using the MRC method. *Spectrochim. Acta A Mol. Biomol. Spectrosc.* **2017**, *181*, 7–12. [[CrossRef](#)] [[PubMed](#)]
46. Djemmo, L.G.; Njanja, E.; Tchieno, F.M.; Ndinteh, D.T.; Ndungu, P.G.; Tonle, I.K. Activated *Hordeum vulgare* L. dust as carbon paste electrode modifier for the sensitive electrochemical detection of Cd<sup>2+</sup>, Pb<sup>2+</sup> and Hg<sup>2+</sup> ions. *Int. J. Environ. Anal. Chem.* **2020**, *100*, 1429–1445. [[CrossRef](#)]
47. Barka, N.; Ouzaouit, K.; Abdennouri, M.; El Makhfouk, M. Dried prickly pear cactus (*Opuntia ficus indica*) cladodes as a low-cost and eco-friendly biosorbent for dyes removal from aqueous solutions. *J. Taiwan. Inst. Chem. Eng.* **2013**, *44*, 52–60. [[CrossRef](#)]
48. Nguyen, Q.H.; Quyen, D.H.; Hoang, T.K.N. A new route of emulsifier-free emulsion polymerization for the preparation of polymer coated magnetite nanoparticles. *Mater. Sci.—Poland* **2014**, *32*, 264–271. [[CrossRef](#)]
49. Devamani, R.H.P.; Alagar, M. Synthesis and characterisation of copper II hydroxide nano particles. *Nano Biomed. Eng.* **2013**, *5*, 116–120. [[CrossRef](#)]
50. Sing, K.S.W. Reporting physisorption data for gas/solid systems with special reference to the determination of surface area and porosity (Recommendations 1984). *Pure Appl. Chem.* **1985**, *57*, 603–619. [[CrossRef](#)]
51. Sidhu, V.; Barrett, K.; Park, D.Y.; Deng, Y.; Datta, R.; Sarkar, D. Wood mulch coated with iron-based water treatment residuals for the abatement of metals and phosphorus in simulated stormwater runoff. *Environ. Technol. Innov.* **2021**, *21*, 101214. [[CrossRef](#)]
52. Tang, C.Y.; Fu, Q.S.; Gao, D.; Criddle, C.S.; Leckie, J.O. Effect of solution chemistry on the adsorption of perfluorooctane sulfonate onto mineral surfaces. *Water Res.* **2010**, *44*, 2654–2662. [[CrossRef](#)] [[PubMed](#)]
53. Appel, C.; Ma, L.Q.; Rhue, R.D.; Kenneley, E. Point of zero charge determination in soils and minerals via traditional methods and detection of electroacoustic mobility. *Geoderma* **2003**, *113*, 77–93. [[CrossRef](#)]
54. Elizondo-Álvarez, M.A.; Uribe-Salas, A.; Bello-Teodoro, S. Chemical stability of xanthates, dithiophosphinates and hydroxamic acids in aqueous solutions and their environmental implications. *Ecotoxicol. Environ. Saf.* **2021**, *207*, 111509. [[CrossRef](#)]
55. Rao, S.R. Flotation Surfactants. In *Surface Chemistry of Froth Flotation*; Springer: New York, NY, USA, 2004; Volume 2, pp. 385–478. [[CrossRef](#)]
56. Jones, M.H.; Woodcock, J.T. *Ultraviolet Spectrometry of Flotation Reagents with Special Reference to the Determination of Xanthate in Flotation Liquors*; Institution of Mining and Metallurgy: London, UK, 1973; p. 25. [[CrossRef](#)]
57. Zhang, H.; Chen, L.; Zhang, D.; Lu, S.; Yu, X. Impact of environmental conditions on the adsorption behavior of radionuclide <sup>63</sup>Ni (II) on  $\gamma$ -Al<sub>2</sub>O<sub>3</sub>. *Colloids Surf. A Physicochem. Eng. Asp. Colloids Surf. A Physicochem. Eng. Asp.* **2011**, *380*, 16–24. [[CrossRef](#)]
58. Li, J.; Chen, S.; Sheng, G.; Hu, J.; Tan, X.; Wang, X. Effect of surfactants on Pb (II) adsorption from aqueous solutions using oxidized multiwall carbon nanotubes. *J. Chem. Eng.* **2011**, *166*, 551–558. [[CrossRef](#)]
59. Coles, C.A.; Yong, R.N. Use of equilibrium and initial metal concentrations in determining Freundlich isotherms for soils and sediments. *Eng. Geol.* **2006**, *85*, 19–25. [[CrossRef](#)]
60. Tran, H.N. Improper estimation of thermodynamic parameters in adsorption studies with distribution coefficient KD (q<sub>e</sub>/C<sub>e</sub>) or Freundlich constant (KF): Considerations from the derivation of dimensionless thermodynamic equilibrium constant and suggestions. *Adsorpt. Sci. Technol.* **2022**, *2022*, 5553212. [[CrossRef](#)]
61. Zhou, X.; Zhou, X. Comments on “Removal of uranium (VI) from aqueous solution by adsorption of hematite”, by Shuibo, X.; Chun, Z.; Xinghuo, Z.; Jing, Y.; Xiaojian, Z.; Jingsong, W.J. *J. Environ. Radioact.* **2019**, *213*, 106106. [[CrossRef](#)]
62. Milonjić, S.K. Comments on “Removal of uranium (VI) from aqueous solution by adsorption of hematite”, by Shuibo, X.; Chun, Z.; Xinghuo, Z.; Jing, Y.; Xiaojian, Z.; Jingsong, W.J. *J. Environ. Radioact.* **2009**, *100*, 921–922. [[CrossRef](#)]
63. Milonjić, S.K. A consideration of the correct calculation of thermodynamic parameters of adsorption. *J. Serb. Chem. Soc.* **2007**, *72*, 1363–1367. [[CrossRef](#)]
64. Bulut, Y.; Tez, Z. Adsorption studies on ground shells of hazelnut and almond. *J. Hazard. Mater.* **2007**, *149*, 35–41. [[CrossRef](#)]
65. Ikefuti, P.V.; Barrozo, L.V.; Braga, A.L.F. An ecological study of the relationship between mean temperature and mortality for stroke in elderly people. In Proceedings of the 27th Conference of the International Society for Environmental Epidemiology, Sao Paulo, Brazil, 30 August–3 September 2015. [[CrossRef](#)]
66. Nibou, D.; Mekatel, H.; Amokrane, S.; Barkat, S.; Trari, M. Adsorption of Zn<sup>2+</sup> ions onto NaA and NaX zeolites: Kinetic, equilibrium and thermodynamic studies. *J. Hazard. Mater.* **2010**, *173*, 637–646. [[CrossRef](#)]
67. Yuh-Shan, H. Review of second-order models for adsorption systems. *J. Hazard. Mater.* **2006**, *136*, 681–689. [[CrossRef](#)]
68. Kumar, D.; Gaur, J.P. Chemical reaction-and particle diffusion-based kinetic modeling of metal biosorption by a *Phormidium* sp.-dominated cyanobacterial mat. *Bioresour. Technol.* **2011**, *102*, 633–640. [[CrossRef](#)] [[PubMed](#)]
69. Onyango, M.S.; Matsuda, H.; Ogada, T. Sorption kinetics of arsenic onto iron-conditioned zeolite. *J. Chem. J. Chem. Eng.* **2003**, *36*, 477–485.
70. Kumar, K.V. Linear and non-linear regression analysis for the sorption kinetics of methylene blue onto activated carbon. *J. Hazard. Mater.* **2006**, *137*, 1538–1544. [[CrossRef](#)] [[PubMed](#)]
71. Wang, J.; Guo, X. Adsorption kinetic models: Physical meanings, applications, and solving methods. *J. Hazard. Mater.* **2020**, *390*, 122156. [[CrossRef](#)] [[PubMed](#)]
72. Senturk, I.; Buyukgungor, H.; Geyikci, F. Biosorption of phenol from aqueous solutions by the *Aspergillus niger* biomass: Comparison of linear and non-linear regression analysis. *Desalin. Water Treat.* **2016**, *57*, 19529–19539. [[CrossRef](#)]

73. Qiu, H.; Lv, L.; Pan, B.C.; Zhang, Q.J.; Zhang, W.M.; Zhang, Q.X. Critical review in adsorption kinetic models. *J. Zhejiang Univ. Sci.* **2009**, *10*, 716–724. [[CrossRef](#)]
74. Karaca, S.; Gürses, A.; Ejder, M.; Açıkıldız, M. Kinetic modeling of liquid-phase adsorption of phosphate on dolomite. *J. Colloid. Interface Sci.* **2004**, *277*, 257–263. [[CrossRef](#)] [[PubMed](#)]
75. Zou, S.P.; Liu, M.; Wang, Q.L.; Xiong, Y.; Niu, K.; Zheng, Y.G.; Shen, Y.C. Preparative separation of echinocandin B from *Aspergillus nidulans* broth using macroporous resin adsorption chromatography. *J. Chromatogr. B.* **2015**, *978*, 111–117. [[CrossRef](#)]
76. Sheha, R.R.; El-Zahhar, A.A. Synthesis of some ferromagnetic composite resins and their metal removal characteristics in aqueous solutions. *J. Hazard. Mater.* **2008**, *150*, 795–803. [[CrossRef](#)]

**Disclaimer/Publisher’s Note:** The statements, opinions and data contained in all publications are solely those of the individual author(s) and contributor(s) and not of MDPI and/or the editor(s). MDPI and/or the editor(s) disclaim responsibility for any injury to people or property resulting from any ideas, methods, instructions or products referred to in the content.